공학박사학위논문

기계 시스템 건전성 평가를 위한 유효독립성 기반 센서 네트워크 디자인 연구

Effective Independence-Based Sensor Network Design for Health Assessment of Engineered Systems

2017년 2월

서울대학교 대학원

기계항공공학부

김 태 진

Abstract

Effective Independence-Based Sensor Network Design for Health Assessment of Engineered Systems

Taejin Kim
Department of Mechanical and Aerospace Engineering
The Graduate School
Seoul National University

The failure of an engineered system not only results in an enormous property loss, but also causes a substantial societal loss. The discipline of prognostics and health management (PHM) recently has received great attention as a solution to prevent unexpected failures of engineered systems. The goal of PHM is to detect anomaly states, to predict potential failures of a system, and to plan an optimal management schedule. PHM is composed of five essential functions: 1) sensing, 2) reasoning, 3) diagnostics, 4) prognostics, and 5) management. The sensing function, in which sensory data is acquired from the system of interest, is a core element needed for cost-effective execution of PHM. The success of the remaining functions in PHM highly depends on the quality of the data obtained by the sensing function.

The research described herein describes the investigation of two original ideas of optimal sensor placement (OSP) for the PHM sensing function. These ideas are aimed to enable cost-effective and robust sensor data acquisition from the system. The first idea is a stochastic effective independence (EFI) method, referred to as an energy-based stochastic EFI method; the proposed method overcomes the drawbacks of existing OSP methods in the sensing function. In Research Thrust 1, the stochastic sensor network design is proposed. It takes the uncertainty of the system into consideration to give more accurate representation of the system than the deterministic sensor network design in the mean sense. Also, the explicit form of the proposed method has the benefit of lower computational requirements, as compared to the sampling-based stochastic approach. In Research Thrust 2, a robust sensor network design that considers the latent failure of the sensor is introduced. The proposed robust sensor network is designed to tolerate the partial failure of the sensor; thus, it contributes to the safety of the sensor network. The proposed method is validated to have accuracy that is comparable to the optimal sensor network design in normal conditions, and higher accuracy for situations in which there is a partial failure of the given sensor network.

Keywords: **Sensor network design**

Effective independence (EFI) method

EigenMap method

Stochastic effective independence method

Robust sensor network design

Student Number: 2011-20702

Contents

List of Tables

List of Figures

Nomenclature

DOF = Degree of Freedom

EFI = Effective Independence Method

FE model = Finite Element model

FIM = Fisher Information Matrix

OSP = Optimal Sensor Placement

PHM = Prognostics and Health Management

RMS = Root Mean Square

ROSP = Robust Optimal Sensor Placement

RUL = Remaining Useful Life

SFEM = Stochastic Finite Element Method

UDDS = Urban Dynamometer Driving Schedule

b = random variable

b^0 = expectation of random variable b

$\mathbf{C}$ = covariance matrix

$\mathbf{E}_D$ = effective independence distribution

$\mathbf{F}_E$ = fractional eigenvalue matrix

f = state function

f^0 = function value evaluated at expectation

$\mathbf{K}$ = stiffness matrix of the FE model

k = number of sensors

$\mathbf{M}$ = mass matrix of the FE model

M = number of data sets

n = dimension of the finite element model

p = probability density function

$\mathbf{q}$ = amplitude corresponding to basis vector of the FE model

$\hat{\mathbf{q}}$ = estimated amplitude corresponding to basis vector of the FE model

$\mathbf{Q}$ = redefined Fisher information matrix

$\mathbf{Q}_0$ = Fisher information matrix

$\mathbf{Q}_{KE}$ = kinetic energy

$\mathbf{Q}_s$ = stochastic Fisher information matrix

$\mathbf{Q}_{SE}$ = strain energy

$\mathbf{Q}^0{}_s$ = Fisher information matrix evaluated at the expectation of the random variable

$\mathbf{W}$ = weight matrix

$\mathbf{w}$ = Gaussian white noise in the signal

$\mathbf{y}$ = arbitrary mechanical signal

$\mathbf{y}_s$ = measured signal

$\hat{\mathbf{y}}$ = regenerated signal

ε = perturbation

$\boldsymbol{\lambda}$ = eigenvalue

μ = mean

σ = variance of signal noise

$\boldsymbol{\Phi}$ = mode shape matrix

$\mathbf{\Phi}_E$ = basis matrix from the covariance matrix

$\mathbf{\Phi}_m$ = mean mode shape matrix

$\mathbf{\Phi}_r$ = mode shape matrix with measured DOF

$\mathbf{\Phi}_s$ = mode shape matrix with measured DOF and selected basis

$\mathbf{\Phi}_v$ = residual mode shape matrix

$\boldsymbol{\psi}$ = eigenvectors of the Fisher information matrix

Chapter 1. Introduction

1.1 Background and Motivation

The failure of a system not only results in enormous damage to the system itself, such as the downtime cost and the restoration cost, failure also causes societal costs, including injury or even loss of human life. As a solution to prevent system failures, recently the field of prognostics and health management (PHM) is getting wide attention [1-5]. The purpose of the PHM is to avoid any kind of failure, and to plan optimal management schedules by estimating the current status, and predicting the remaining useful life (RUL) of a system.

The PHM is composed of four functions; specifically, the sensing, reasoning, prognostics, and management functions. In the sensing function, sensors are placed on the system to obtain the proper data that gives relevant information for the reasoning function. In the following stage of reasoning, the obtained data is analyzed to verify the current conditions of the system. Then, the prognostics function predicts the RUL based on the past and current conditions that were verified during the reasoning function. Finally, using all the information up to the prognostics function, proper decisions about the operation and maintenance are made as part of the management function.

As seen in the overall process of PHM, sensing is the beginning step of the whole process. Each subsequent step depends on the sensing step. Therefore, proper sensing is very important for successful PHM. If successful implementation of this step is possible, the following diagnostics steps can be achieved much more efficiently, or with very simple algorithms. That is, if the sensors can be set up to accurately reveal the difference between normal and abnormal conditions, there is no need for expensive algorithms. In contrast, if the measured data is not relevant to the target failure, even complicated and expensive algorithms may not work.

Good sensing can be determined by answering two questions: What should be measured? and how should this data be measured? There are many signals coming out of a system, such as the vibration, pressure, temperature, and so on. Among these signals, what should be measured must be the signal(s) that best represent(s) the health conditions of the system. For example, in a battery system, vibration gives very little information about the system's health; however, the open circuit voltage is a good indicator of health [6-8]. In contrast, in a structural system, vibration does work as a good indicator of health [9-11]; however, voltage is not a health indicator at all. This example reveals that the type of signal that should be measured is highly dependent on the system. Since the choice of signal type is system dependent, it must be studied individually for each system. Likewise, it is out of the scope of this study to consider any general approach for sensor placement. Once the relevant type of

signal is determined, then the locations of the sensors must be chosen. The sensors must be placed to extract the maximum information from the system. Maximizing information also means avoiding duplication of information from sensors. One obvious example of duplicated information is to put sensors on the same spot, so that they measure the exactly the same information. However, duplicated information is not just limited to this type of case, it also can occur in the case of sensors that are not in close proximity. These concepts will be discussed in the following chapter. Based on this measure of information, the various approaches for sensor placement will be discussed.

1.2 Research Objectives and Scopes

The research described in this work involves two research objectives, as follows.

Objective 1 – Stochastic sensor placement

Uncertainty always exists in the real world, and it affects the results of sensor placement in PHM. However, most of the sensor placement methods available to date are focused on the deterministic aspects of the system. To enhance the performance of the sensor network design, sensors must be placed to maximize the information that contains uncertainty. To this end, this research explores a sensor

placement method for a system with random properties. The existing sensor placement method, called the effective independence method (EFI), is modified in this research to its stochastic version. Through this method, more information can be obtained (on average) than can be obtained by the deterministic approach.

Objective 2 – Robust sensor placement

In spite of the importance of the sensing system to PHM, the robustness of the sensor network design has not yet been seriously considered by researchers. The failure of one sensor could collapse the overall estimation algorithm or result in very poor estimation. Accordingly, a sensor network design that can deal with a possible malfunction is required. The redundant use of sensors has so far been considered the only possible option for enhancing robustness. However, this approach is not cost-effective, and does not help obtain more information, despite the use of additional sensors. In this study, we propose a sensor network design that improves both the robustness and the amount of information gathered. The proposed method is applied to and validated with a battery pack system where knowledge of the temperature distribution is of importance for safety and system management. The proposed sensor network design gives an accurate estimation of the thermal map as well as the robustness.

1.3 Dissertation Overview

This dissertation is organized as follows. Chapter 2 reviews the current sensor network design methods related to the research topics, including the effective independence method, the energy-based method, and the eigenmap method. Chapter 3 presents the proposed stochastic sensor placement method that expands the effective independence method to a stochastic version. In Chapter 4, the sensor network design that considers the failure of the sensor is explained. A battery pack study is employed to demonstrate the robustness of the proposed sensor network design. Finally, Chapter 5 discusses the contributions of the studies and potential future research directions. The challenges, objectives, and expected benefits of the proposed research are summarized in Table 1-1.

Table 1-1 Challenges, objectives, and benefits of this research

Challenges	• No available analytic approach for stochastic sensor network design • Failure of a sensor collapses the performance of the whole sensor network • Low detectability for fault conditions
Objectives	• Develop an analytic solution for stochastic sensor network design • Develop a robust sensor network design that considers sensor malfunctions • Sensor network design for diagnostics by enhancing the detectability of the fault conditions
Expected benefits	• Analytic solution for stochastic sensor network design • Computational cost savings through the new method • A relevant solution for practical use • Enhancement of the robustness of the sensor network, making it compatible with improved failure detection • Securing the buffering time before maintenance of the system • Enhanced detectability for a specific fault condition • Reduced work in the following PHM steps by obtaining abundant information

Chapter 2. Literature Review

This chapter provides a background on the associated knowledge related to this dissertation. Section 2.1 introduces the linear independence of a system as a measure of the information. The following sections discuss how to maximize the linear independence, or the amount of information, and introduce a solution of the EFI method. The EFI method is used to measure the raw signal from sensors, and it can be modified for energy-based sensor placement, which is described in Section 2.3. In the last section, the eigenmap method is introduced. Unlike the EFI method, which is based on the finite element (FE) model, the eigenmap method utilizes the data.

2.1 Linear Independence of a System

As described in Chapter 1, the performance of PHM largely depends on the quality of the information measured. In this section, a measure of the information is introduced, and using this measure, sensor locations are found such that there will be no duplicated information. First, to see how the information is measured, let's assume that the behavior of the whole system is in question. In this case, we try to estimate the system state based on the given number of sensors, or given data at specific locations.

To get an idea on estimating the whole system, let's first look at how an arbitrary signal is made up. An arbitrary mechanical signal can be decomposed into the mode shapes and the corresponding amplitudes, as in Eq.(1) [12].

$$\mathbf{y} = \mathbf{\Phi q} + \mathbf{w} \tag{1}$$

where y is an arbitrary mechanical signal described by an n×1 vector, $\mathbf{\Phi}$ is an n×n mode shape matrix obtained from the stiffness matrix of an FE model, $\mathbf{q}$ is an n×1 target modal coordinate or amplitude corresponding to the mode shape, and $\mathbf{w}$ is the Gaussian white noise with variance σ. If each degree-of-freedom (DOF) of the FE model is known or measurable, the mode shapes are linearly independent, as shown in Figure 2-1(a). However, if the sensors are placed only in limited locations, which is the usual case, only the measured DOFs are known, and they could be linearly dependent, as shown in Figure 2-1(b). In this case, these reduced mode shapes contain the duplicated information to reconstruct the signal. Thus, the sensors must be placed to avoid these linear dependences, and to maximize the linear independence. The details to accomplish this are explained in the following section.

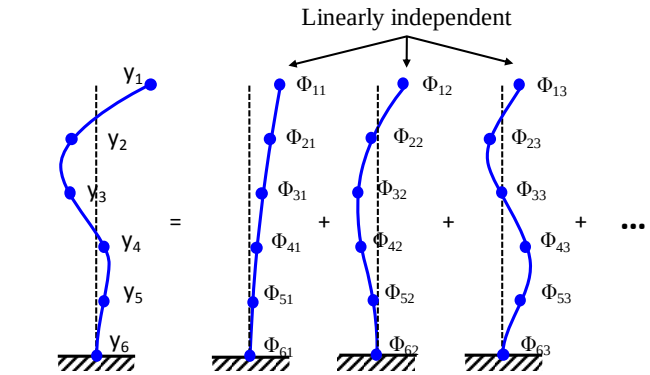

(a)

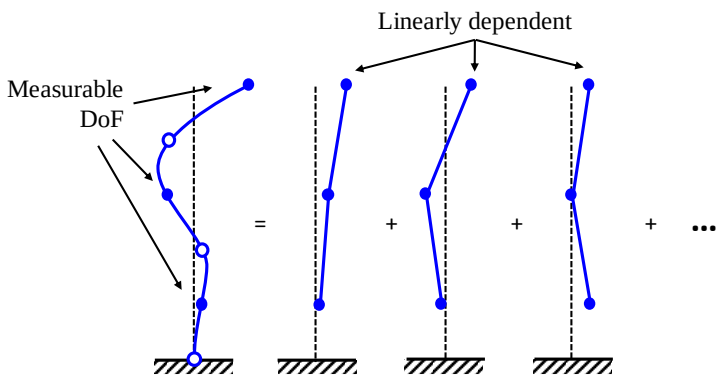

(b)

Figure 2-1 Linear independence of the system according to the sensor locations: (a) If the data is measurable in every DOF, the mode shapes are linearly independent, (b) if the data is partially measurable, the mode shapes could be linearly dependent, depending on the measured DOFs.

2.2 Model-based Sensor Placement Method: Effective Independence Method

Since the mode shape matrix in Eq.(1) reflects the characteristics of the system itself, it is obtainable once the system is defined. Then it is the amplitude, **q** that determines a specific signal, **y**. That is, knowing the signal **y** is equivalent to knowing amplitude, **q**. Therefore, estimation of the entire *y* from the limited information of **y** is identical with estimation of **q**. From the best linear unbiased estimator, we have the estimation of **q** as follows [13, 14]:

$$\hat{\mathbf{q}} = \left(\boldsymbol{\Phi}_s^{\mathrm{T}}\boldsymbol{\Phi}_s\right)^{-1}\boldsymbol{\Phi}_s^{\mathrm{T}}\mathbf{y}_s \tag{2}$$

where $\mathbf{y}_s$ is a k×1 (k<n) vector that has partial elements of the target signal **y**, that is, the measured signal, and $\boldsymbol{\Phi}_s$ is the reduced k×k mode shape matrix. Then the target signal is estimated using $\hat{\mathbf{q}}$ and $\boldsymbol{\Phi}_r$, an n×k mode shape matrix. The estimated signal $\hat{\mathbf{y}}$ is a signal regenerated with some of the mode shapes and the corresponding estimated amplitude.

$$\hat{\mathbf{y}} = \boldsymbol{\Phi}_r\hat{\mathbf{q}}\,. \tag{3}$$

Eq.(3) describes how to estimate the target signal when the partial signal is measured. Now the problem is how to select the measured locations for the best

estimation of **q**. The answer to this is attained by minimizing the variance of the estimation, which is given by

$$\mathbf{P} = E[(\mathbf{q}-\hat{\mathbf{q}})(\mathbf{q}-\hat{\mathbf{q}})^T] = \left[\frac{1}{\sigma^2}\mathbf{\Phi}^T\mathbf{\Phi}\right]^{-1} = \mathbf{Q}_0{}^{-1}. \quad (4)$$

In this equation, the quadratic form of $\mathbf{\Phi}$ or, in other words, $\mathbf{Q}_0$ is called the Fisher information matrix (FIM). If the measurement noise is uncorrelated and identical, the Fisher information matrix can be equivalently expressed as $\mathbf{Q} = \mathbf{\Phi}^T\mathbf{\Phi}$. The minimization of the covariance matrix is equivalent to maximizing the Fisher information matrix. The proper norm to measure the Fisher information matrix is its determinant, because the determinant of the Fisher information matrix is largest for the best linear estimation [14, 15].

If the determinant of the FIM is zero, the mode shape vectors are linearly dependent. Conversely, to have the maximum linear independence, the determinant of the FIM should be maximized. To this end, the fractional eigenvalue matrix is calculated as

$$\mathbf{F}_E = [\mathbf{\Phi\psi}] \otimes [\mathbf{\Phi\psi}] \boldsymbol{\lambda}^{-1} \quad (5)$$

where $\boldsymbol{\psi}$ are the eigenvectors of **Q**; $\boldsymbol{\lambda}$ are the associated eigenvalues; and $\otimes$ is the term-by-term matrix multiplication. The component in the *i*th row and the *j*th column

of the matrix $\mathbf{F}_E$ is the contribution of the *i*th DOF to the *j*th eigenvalue. Then, the summation of each column gives the effective independence distribution, E_D

$$\mathbf{E}_D = [\boldsymbol{\Phi}\boldsymbol{\psi}] \otimes [\boldsymbol{\Phi}\boldsymbol{\psi}] \boldsymbol{\lambda}^{-1} \cdot \mathbf{1} \tag{6}$$

where **1** is the vector where the vector's elements are all ones. The *i*th entity of $\mathbf{E}_D$ is the contribution of the corresponding DOF to the linear independence of the modal shape matrix. For each iteration, the DOF that has the lowest value of $\mathbf{E}_D$ is eliminated, and the process is repeated until the desired number of DOFs remains. The algorithm is summarized in Table 2-1 as a pseudo-code.

Table 2-1 Pseudo-code for the effective independence method

Step	Pseudo code
1	**initialize** B = {1, …, N}, D = {1, …, K}
2	**repeat**
3	Set $\boldsymbol{\Phi}_r \leftarrow \boldsymbol{\Phi}$[B, D]
4	$\mathbf{Q} = \boldsymbol{\Phi}_r^T \boldsymbol{\Phi}_r$
5	Find eigenvalues λ and eigenvectors $\boldsymbol{\psi}$ of $\mathbf{Q}$
6	Calculate $\mathbf{F}_E = [\boldsymbol{\Phi}_r\boldsymbol{\psi}] \otimes [\boldsymbol{\Phi}_r\boldsymbol{\psi}]\, \boldsymbol{\lambda}^{-1}$
7	Calculate $\mathbf{E}_D = [\boldsymbol{\Phi}_r\boldsymbol{\psi}] \otimes [\boldsymbol{\Phi}_r\boldsymbol{\psi}]\, \boldsymbol{\lambda}^{-1} \cdot \mathbf{1}$
8	$B \leftarrow B \cap \{n\}^c$: Remove *n*th DOF corresponding to the least value of $\mathbf{E}_D$ from B.
9	**until** |B| = K
10	**return** B
11	**end**

2.3 Energy-Based Sensor Placement Method

In the previous section, the quantity we tried to reconstruct was the raw signal that is directly measured by the sensors. However, sometimes the energy of the system is a useful quantity to determine the status of the system [16-18]. Here, we introduce an energy-based sensor placement method that maximizes the energy of the measured mode shape. It is nothing but a small modification of the EFI method.

The kinetic energy of the system is expressed as

$$\mathbf{Q}_{KE} = \boldsymbol{\Phi}^{\mathrm{T}}\mathbf{M}\boldsymbol{\Phi} = \xi^{\mathrm{T}}\xi \tag{7}$$

where **M** is the mass matrix. In the above equation, the kinetic energy equation is modified as $\xi^{\mathrm{T}}\xi$ to have the same quadratic form with the FIM, so the same procedure used in the EFI method can be applied for energy-based sensor placement. In Eq. (7), the form of ξ is defined by decomposing the mass matrix. One way of decomposition is to use the Cholesky decomposition; in this case, ξ is defined as $\xi = \mathbf{D}\boldsymbol{\Phi}$ where $\mathbf{M} = \mathbf{D}^{\mathrm{T}}\mathbf{D}$, and **D** is the lower triangular matrix. For other decompositions and their effects, one can refer to [19].

In the same way, the strain energy-based sensor placement is possible by replacing the mass matrix with the stiffness matrix [20, 21].

$$\mathbf{Q}_{SE} = \mathbf{\Phi}^{\mathrm{T}}\mathbf{K}\mathbf{\Phi} = \xi^{\mathrm{T}}\xi \tag{8}$$

Here **K** is the stiffness matrix. As mentioned, the **K** is also decomposed in various ways.

2.4 Data-Based Sensor Placement Method: EigenMap Method

In the EFI method, the mode shapes that are the basic building blocks for any signal are used to find the sensor locations. Since the mode shapes are obtained as the eigenvectors of the stiffness matrix from the FE physical model, it was called the model-based approach. As known from linear algebra, there also exist other forms of basis vectors. This section introduces the EigenMap method that attains the basis vectors from the data set [22-24], so it can be called the data-based method in comparison to the model-based EFI method. The only difference between the EigenMap method and the EFI method is that they are using different basis vectors; this difference characterizes each method.

The basis vectors in the EigenMap method are obtained from the covariance matrix, **C**, of the *M* data set $y^m\}_{m=1}^{M}$. The *i*th row and *j*th column component of **C** are defined as

$$\mathbf{C}[i, j] = \mathrm{Cov}(y_i, y_j) = \mathrm{E}[(y_i - \mu_i)(y_j - \mu_j)] \tag{9}$$

where μ_i is the mean of the ith component of y^m. Then, the matrix $\mathbf{\Phi}_E$ where the ith column corresponds to the ith largest eigenvector of the covariance matrix plays the role of the mode shape matrix, as in the EFI method. The rest of the procedure to find the DOFs that have the highest contribution to the linear independence is the same as in the EFI method.

Since both the EFI method and the EigenMap method are based on the basis vectors of the system, they can estimate any kind of signal to some extent. However, the difference is that the EFI method shows good estimation capability in general, while the EigenMap method shows very accurate results for system behavior similar to the training data, but is less accurate for other cases. This difference is schematically shown in Figure 2-2. The choice of the methods could be determined according to the operating condition of the system. If the system is operating under restricted conditions, the EigenMap method could give accurate estimation results with a smaller number of sensors. On the other hand, if the operating conditions are not restricted to particular operating conditions, the use of the EFI method will give better results.

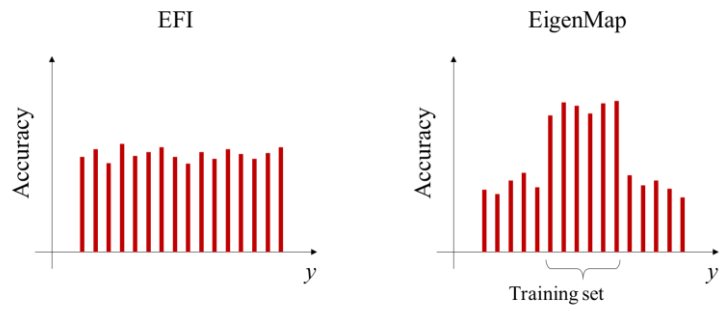

Figure 2-2 Schematic performance comparison of EFI and the EigenMap method.

Chapter 3. Stochastic Sensor Network Design

This Chapter discusses optimal sensor placement under parametric uncertainties. The EFI method is reformulated from the stochastic view. The resultant formula for stochastic EFI contains the deterministic term, which has the same form with the deterministic EFI, and an additional stochastic term. The stochastic term can be calculated with the help of the stochastic finite element method (SFEM). The developed method is expanded to the energy-based OSP method.

3.1 Stochastic Finite Element Method

3.1.1 Principle of Stochastic Perturbation

The uncertainty of the OSP problem can be quantified with probabilistic moments using SFEM. In this research, the perturbation-based method is adapted to calculate the probabilistic moments [25-28]. The perturbation-based method finds the stochastic moments of the target function by expanding the state function of the random variables using the Taylor series. That is, for a random variable, b, the Taylor series expansion of state function $f(b)$ is

$$f(b) = f^0 + \sum_{n=1}^{\infty} \frac{1}{n!} \varepsilon^n \frac{\partial^n f(b)}{\partial b^n} (\Delta b)^n \tag{10}$$

where f^0 denotes the function value evaluated at the expectation b^0; $\varepsilon\Delta b = \varepsilon\,(b - b^0)$ is the first variation of b for a perturbation with a given small parameter ε. The expectation of the target function with the probability density $p(b)$ is

$$\begin{aligned} E[f(b);b] &= \int_{-\infty}^{+\infty} f(b)p(b)\mathrm{d}b \\ &= f^0 + \sum_{n=1}^{\infty} \frac{1}{n!}\varepsilon^n \frac{\partial^n f(b)}{\partial b^n}\mu_n(b) \end{aligned} \tag{11}$$

In the last equation, the mth central moment, μ_m is

$$\mu_m(f(b);b) = \int_{-\infty}^{+\infty} (f(b) - E)^m p(b)\mathrm{d}b\,. \tag{12}$$

For example, the second-order central moment, also called variance, up to fourth order accuracy is

$$\mathrm{Var}(f(b)) \approx \varepsilon^2 \left(\frac{\partial f}{\partial b}\right)^2 \mu_2(b) + \varepsilon^4 \left\{\frac{1}{4}\left(\frac{\partial^2 f}{\partial b^2}\right)^2 + \frac{1}{3}\frac{\partial^3 f}{\partial b^3}\frac{\partial f}{\partial b}\right\}\mu_4(b) \tag{13}$$

For the higher-order moments up to higher-order accuracy, refer to [26]. The nth order partial derivatives in the expectation and the moment equation are obtained by numerically solving the variational formulation of the linear structural system equation.

3.1.2 Stochastic Eigenvalue Problem

The stochastic characteristics of the mode shape matrix are obtained by solving the eigenproblem of the mass and stiffness matrix. The expanded mass and stiffness matrix by the Talyor series is substituted into the variational formulation and the same order of perturbation ε is equated to have the following eigenvalue problem [25, 29]:

Zeroth order:

$$\left[K^0_{\alpha\beta}(b^0_\rho) - \lambda^0_\beta(b^0_\rho) M^0_{\alpha\beta}(b^0_\rho)\right]\phi^0_\beta(b^0_\rho) = 0 \tag{14}$$

First order:

$$\left[K^0_{\alpha\beta}(b^0_\rho) - \lambda^0_\beta(b^0_\rho) M^0_{\alpha\beta}(b^0_\rho)\right]\phi^{,\rho}_\beta(b^0_\rho) = -\left[K^{,\rho}_{\alpha\beta}(b^0_\rho) - \lambda^{,\rho}_\beta(b^0_\rho) M^0_{\alpha\beta}(b^0_\rho) - \lambda^0_\beta(b^0_\rho) M^{,\rho}_{\alpha\beta}(b^0_\rho)\right]\phi^0_\beta(b^0_\rho) \tag{15}$$

where M and K are the mass and stiffness matrix; λ_β and ϕ_β are the system eigenvalue and the corresponding eigenvector; and the superscript $(\cdot)^{,\rho}$ indicates the first-order derivative with respect to the random variable b_ρ. To know the statistics of the eigenvalue and eigenvector, refer to [25]. Then, the first-order accurate cross-covariance for the α-th component of the α_p-th eigenvector and the β-th component of the β_p-th eigenvector is calculated as

$$\mathrm{Cov}(\phi^0_{\alpha(\alpha_p)}, \phi^0_{\beta(\beta_p)}) = \phi'^{\rho}_{\alpha(\alpha_p)} \phi'^{\sigma}_{\beta(\beta_p)} \mathrm{Cov}(b_\rho, b_\sigma) \tag{16}$$

This stochastic moment is used for the stochastic EFI in the following section.

3.2 Stochastic Effective Independence Method

The EFI method is analyzed considering the parametric uncertainty. In Eq.(1) the uncertainty of the output *y* comes from the measurement noise *w*. However, in reality, the target mode shape $\mathbf{\Phi}$ also has uncertainty that comes from the parametric uncertainties, such as Young's modulus. Thus, a random sample of $\mathbf{\Phi}$ can be expressed as the sum of mean $\mathbf{\Phi}_\mathrm{m}$ and residual $\mathbf{\Phi}_\mathrm{v}$,

$$\mathbf{\Phi} = \mathbf{\Phi}_m + \mathbf{\Phi}_v \tag{17}$$

Then Eq.(1) is described as

$$\mathbf{y} = \mathbf{\Phi}_m \mathbf{q} + \mathbf{\Phi}_v \mathbf{q} + \mathbf{w} \tag{18}$$

In this equation, $\mathbf{\Phi}_m$ is deterministic, and $\mathbf{\Phi}_v\mathbf{q}+\mathbf{w}$ is random. Comparing Eq.(18) with Eq.(1), $\mathbf{\Phi}_v\mathbf{q}+\mathbf{w}$ can be interpreted as the measurement noise. Hence, the noise variance term of the initial FIM in Eq.(4) is no longer considered constant. Therefore, the FIM is affected by the variance of $\mathbf{\Phi}$. From this perspective, we see that a DOF

that largely contributes to the linear independence of the mode shapes cannot always be included in the set of sensor locations if its variance is considered. There might be a balancing point between linear independence and variance that maximizes the determinant of the FIM, on average.

To analyze the effect of the uncertainty of the mode shape matrix and to evaluate the optimal sensor location, the mode shape matrix is expressed as in Eq.(17). Then, the FIM is

$$\mathbf{Q}_s = \left(\boldsymbol{\Phi}_m + \boldsymbol{\Phi}_v\right)^T \left(\boldsymbol{\Phi}_m + \boldsymbol{\Phi}_v\right) \tag{19}$$

Instead of integrating the randomness into the measurement noise, the randomness is maintained in the mode shape matrix to keep the same form of the FIM with the deterministic EFI method. In this case, the variance of noise is stationary and hence ignored in the FIM. The fractional eigenvalue matrix is obtained as

$$\mathbf{F}_E = \left[\left(\boldsymbol{\Phi}_m + \boldsymbol{\Phi}_v\right)\left(\boldsymbol{\psi}_m + \boldsymbol{\psi}_v\right)\right] \otimes \left[\left(\boldsymbol{\Phi}_m + \boldsymbol{\Phi}_v\right)\left(\boldsymbol{\psi}_m + \boldsymbol{\psi}_v\right)\right] \left(\boldsymbol{\lambda}_m + \boldsymbol{\lambda}_v\right)^{-1} \tag{20}$$

The eigenvalue and the eigenvector of $\mathbf{Q}_s$ are expressed as $(\boldsymbol{\lambda}_m + \boldsymbol{\lambda}_v)$ and $(\boldsymbol{\psi}_m + \boldsymbol{\psi}_v)$, respectively, since they are also random from the randomness of $\mathbf{Q}_s$. To reduce the complexity, those eigenpairs are approximated using the first-order, perturbation-

based stochastic finite element method [25], which is obtained by solving the eigenproblem:

$$\left[\mathbf{Q}_s^0 - \boldsymbol{\lambda}_m \mathbf{I}\right]\boldsymbol{\psi}_m = 0 \tag{21}$$

$\boldsymbol{Q}^0_s$ is the value evaluated at the expectation of the random variable. Then, the fractional eigenvalue matrix becomes

$$\mathbf{F}_E = \left[\left(\boldsymbol{\Phi}_m + \boldsymbol{\Phi}_v\right)\boldsymbol{\psi}_m\right] \otimes \left[\left(\boldsymbol{\Phi}_m + \boldsymbol{\Phi}_v\right)\boldsymbol{\psi}_m\right] \boldsymbol{\lambda}_m^{-1} \tag{22}$$

Figure 3-1 shows the schematic representation of Eq.(22). A sample of the row of $\boldsymbol{\Phi}$ has a probabilistic distribution where its mean is located at $\boldsymbol{\Phi}_m$ and its residual is $\boldsymbol{\Phi}_v$. This row vector of the mode shape matrix is transformed by the mean eigenvector $\boldsymbol{\psi}_m$ to the eigenvector space, called absolute identification space. Then, the magnitude of the transformed vector is measured by the term-by-term multiplication and normalized by the mean eigenvalue $\boldsymbol{\lambda}_m$ to compare the transformed vector based on the same measure.

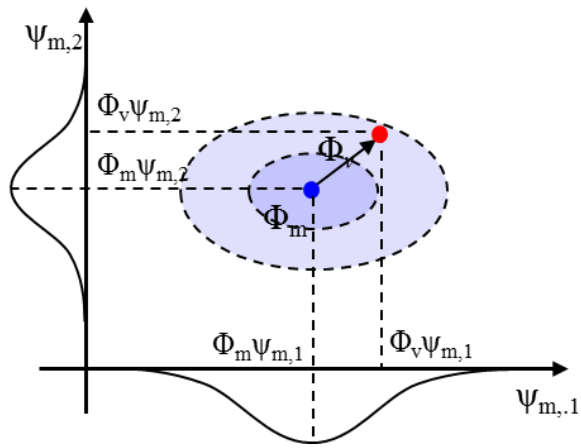

Figure 3-1 Transformation of the row of the mode shape matrix ($\boldsymbol{\Phi}_m$) to the absolute identification space.

$$\begin{aligned}\mathrm{E}\left[\mathbf{F}_E\right] &= \mathrm{E}\left[\left[\left(\boldsymbol{\Phi}_m+\boldsymbol{\Phi}_v\right)\boldsymbol{\psi}_m\right]\otimes\left[\left(\boldsymbol{\Phi}_m+\boldsymbol{\Phi}_v\right)\boldsymbol{\psi}_m\right]\boldsymbol{\lambda}_m^{-1}\right] \\ &= \left[\boldsymbol{\Phi}_m\boldsymbol{\Psi}_m\right]\otimes\left[\boldsymbol{\Phi}_m\boldsymbol{\Psi}_m\right]\boldsymbol{\lambda}_m^{-1}+2\mathrm{E}\left[\left[\boldsymbol{\Phi}_m\boldsymbol{\Psi}_m\right]\otimes\left[\boldsymbol{\Phi}_v\boldsymbol{\Psi}_m\right]\right]\boldsymbol{\lambda}_m^{-1} \\ &\quad +\mathrm{E}\left[\left[\boldsymbol{\Phi}_v\boldsymbol{\Psi}_m\right]\otimes\left[\boldsymbol{\Phi}_v\boldsymbol{\Psi}_m\right]\right]\boldsymbol{\lambda}_m^{-1}\end{aligned} \tag{23}$$

The expectation of the second term in Eq.(23) is

$$\mathrm{E}\left[\left[\boldsymbol{\Phi}_m\boldsymbol{\Psi}_m\right]\otimes\left[\boldsymbol{\Phi}_v\boldsymbol{\Psi}_m\right]\right]\boldsymbol{\lambda}_m^{-1}=\left[\boldsymbol{\Phi}_m\boldsymbol{\Psi}_m\right]\otimes\mathrm{E}\left[\boldsymbol{\Phi}_v\right]\boldsymbol{\Psi}_m\boldsymbol{\lambda}_m^{-1} \tag{24}$$

The expectation of $\boldsymbol{\Phi}_v$ is zero; with the assumption of a symmetric distribution of $\boldsymbol{\Phi}$, Eq.(24) vanishes. The expectation of the last term in Eq.(23) is

$$\mathrm{E}\left[\left[\left[\boldsymbol{\Phi}_v\boldsymbol{\Psi}_m\right]\otimes\left[\boldsymbol{\Phi}_v\boldsymbol{\Psi}_m\right]\right]_{ij}\right]=\sum_k\sum_l\mathrm{Cov}\left[\Phi_{v,ik},\Phi_{m,il}\right]\Psi_{m,kj}\Psi_{m,lj} \tag{25}$$

If there is no correlation between the element of $\boldsymbol{\Phi}_v$, (for example, Young's modulus of a truss element is not affected by, or independent from the other elements), Eq.(25) becomes

$$\mathrm{E}\left[\left[\boldsymbol{\Phi}_v\boldsymbol{\Psi}_m\right]\otimes\left[\boldsymbol{\Phi}_v\boldsymbol{\Psi}_m\right]\right]=\mathrm{Var}\left[\boldsymbol{\Phi}_v\right]\left[\left[\boldsymbol{\Psi}_m\right]\otimes\left[\boldsymbol{\Psi}_m\right]\right] \tag{26}$$

In Eq.(26), the Var[$\boldsymbol{\Phi}_v$] indicates the elementary variance of $\boldsymbol{\Phi}_v$. In conclusion, the expectation of $\mathbf{F}_E$ is

$$\mathrm{E}\left[\mathbf{F}_E\right]=\left[\boldsymbol{\Phi}_m\boldsymbol{\Psi}_m\right]\otimes\left[\boldsymbol{\Phi}_m\boldsymbol{\Psi}_m\right]\boldsymbol{\lambda}_m^{-1}+\mathrm{Var}\left[\boldsymbol{\Phi}_v\right]\left[\left[\boldsymbol{\Psi}_m\right]\otimes\left[\boldsymbol{\Psi}_m\right]\right]\boldsymbol{\lambda}_m^{-1} \tag{27}$$

In this equation, the first term is the same as the deterministic EFI evaluated at the expectation, and the second term contains the effect of the variance on FIM. Finally, the summation of the column vector of the E[$\mathbf{F}_E$], the stochastic effective independence distribution $\mathbf{E}_{D,SEFI}$, represents the contribution of a DOF to the determinant of the FIM.

$$\mathbf{E}_{D,SEFI} = \mathrm{E}\left[\mathbf{F}_E\right] = \left[\boldsymbol{\Phi}_m \boldsymbol{\Psi}_m\right] \otimes \left[\boldsymbol{\Phi}_m \boldsymbol{\Psi}_m\right] \boldsymbol{\lambda}_m^{-1} \cdot \mathbf{1} + \mathrm{Var}\left[\boldsymbol{\Phi}_v\right] \left[\left[\boldsymbol{\Psi}_m\right] \otimes \left[\boldsymbol{\Psi}_m\right]\right] \boldsymbol{\lambda}_m^{-1} \cdot \mathbf{1} \qquad (28)$$

Then, the rest of the procedure is identical to the procedure used for deterministic EFI, described in Section 2. That is, the DOF with the lowest value of $\mathbf{E}_{D,SEFI}$ is removed at each iteration until the number of the remaining DOFs reaches the given number of sensors.

As an example, consider the following probabilistic mode shape matrix $\boldsymbol{\Phi}$ composed of the mean $\boldsymbol{\Phi}_\mathrm{m}$ and the deviation $\boldsymbol{\Phi}_\mathrm{v}$. The elements of the mode shape matrix have the probabilistic distribution function following the Gaussian distribution, where its mean and deviation are

$$\mathrm{E}\left[\boldsymbol{\Phi}\right] = \boldsymbol{\Phi}_m = \begin{bmatrix} 5 & 1 \\ 4 & 4 \\ 1 & 1 \end{bmatrix} \quad \text{and} \quad \mathrm{Var}\left[\boldsymbol{\Phi}\right] = \mathrm{Var}\left[\boldsymbol{\Phi}_v\right] = \begin{bmatrix} 0.5^2 & 0.1^2 \\ 0.4^2 & 0.4^2 \\ 0.3^2 & 0.3^2 \end{bmatrix}.$$

Each row and column of $\boldsymbol{\Phi}$ corresponds to the DOF and the mode shape, respectively. Transformation of each row of $\boldsymbol{\Phi}$ to the absolute identification space generated by the mean eigenvectors $\boldsymbol{\psi}_m$ of the FIM is shown in Figure 3-2. In the figure, the transformed vector $\Phi_i\psi_m$ from the ith row of $\boldsymbol{\Phi}$ by the conventional deterministic approach is indicated by the arrow named $\rho_{i,det}$. Furthermore, to compare this deterministic result with the stochastic result, 1,000 samples of $\boldsymbol{\Phi}$ were generated according to its PDF and transformed to the eigenvector space of the FIM. The result is shown as clustered points around each tip of the arrow, and named $\rho_{i,MCS}$. From Eq.(6), the squares length of the transformed vector is related to the linear independency, and it will be affected by the randomness as observed in the figure. To see this, the effective independence distribution, $\mathbf{E}_D$ is calculated using three methods, namely, the deterministic method, the mean value of MCS method, and the proposed stochastic EFI method; these methods are, respectively

$$\mathbf{E}_{D,\text{det}} = \begin{bmatrix} 1 \\ 0.9412 \\ 0.0588 \end{bmatrix}, \quad \mathbf{E}_{D,\text{MCS}} = \begin{bmatrix} 0.9876 \\ 0.9341 \\ 0.0783 \end{bmatrix}, \text{ and } \quad \mathbf{E}_{D,\text{SEFI}} = \begin{bmatrix} 1.0022 \\ 0.9434 \\ 0.0787 \end{bmatrix}$$

The elements of $\mathbf{E}_D$ represent the contribution of corresponding DOFs to the linear independence. From the 3rd row of $\mathbf{E}_{D,\text{det}}$, and $\mathbf{E}_{D,\text{MCS}}$, we see that the randomness truly affects the contribution of DOFs to the linear independence, which could change the selection of the sensor. Also, we see that the randomness is

accurately captured by the stochastic EFI method. Hence, the stochastic EFI method will help to select the optimal sensor location under uncertainty.

The result by MCS in the example is used as a benchmark test to compare the accuracy of the stochastic property by the proposed method. However, the MCS method cannot be applied in this way because the stochastic property for the mode shape matrix is not known; it is computationally expensive to obtain it at every iteration of the EFI method. Instead, the MCS method is used to generate random samples, and to select the sensor locations for each samples [20]. Then, the most frequently selected sensors out of all samples are determined as the final sensor locations. This approach, however, contains the possibility that sensors with a low contribution to the linear independence are selected instead of those with a higher one. This will be shown and discussed in Section 3.4.

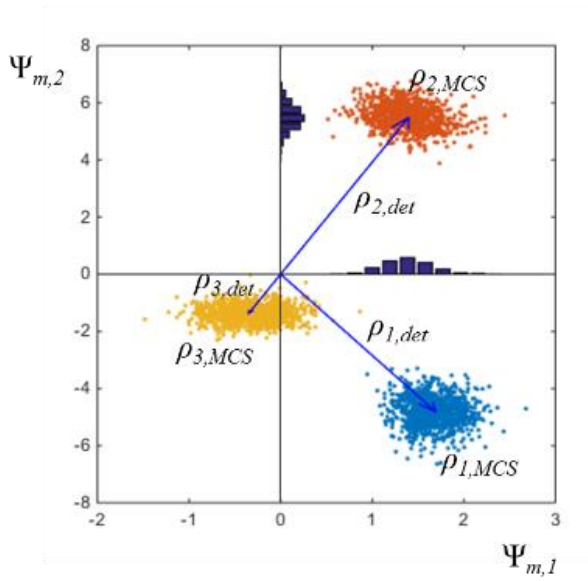

Figure 3-2 Example of the transformation of the row of the mode shape matrix ($\boldsymbol{\Phi}_m$) to the absolute identification space. The arrow indicates the deterministic transformation and the point cluster indicates the probabilistic transformation generated by the MCS method.

3.3 Energy-Based Stochastic EFI Method

The EFI method is expanded to the energy-based method by adapting the mass and stiffness matrix into the FIM. The FIM is then expressed as

$$\mathbf{Q}_E = \mathbf{\Phi}^{\mathrm{T}} \mathbf{W} \mathbf{\Phi} \tag{29}$$

If the weight matrix **W** is the mass matrix, as in Eq.(7), it is the kinetic energy equation; if **W** is the stiffness matrix, it is the strain energy equation. For the energy method, the FIM is newly defined as

$$\mathbf{Q}_E = \zeta^{\mathrm{T}} \zeta \qquad \text{where} \quad \zeta = \mathbf{C}\mathbf{\Phi} \tag{30}$$

Here, the weight **W** is decomposed by the Cholesky decomposition as $\mathbf{W}=\mathbf{C}^{\mathrm{T}}\mathbf{C}$. The decomposition of the weight matrix can be executed in several different ways, such as $\mathbf{W} = \sqrt{\mathbf{C}}\sqrt{\mathbf{C}}$. To check other decomposition options and their effects on the results, refer to [19].

Once the FIM is defined, the rest of the procedure is identical to the EFI method. The only difference is that Φ is replaced by ζ. Then, the mean and the covariance of ζ are calculated as

$$\zeta_m = \mathbf{C}\mathbf{\Phi}_m \tag{31}$$

$$\mathrm{Cov}\left[\zeta_{v,ij}\right] = \mathbf{C}\mathrm{Cov}\left[\Phi_{v,ij}\right]\mathbf{C}^{\mathrm{T}} \tag{32}$$

The resultant expectation of the fractional eigenvalue matrix $\mathbf{F}_E$ for the energy-based method is

$$\mathrm{E}\left[\mathbf{F}_E\right] = \left[\boldsymbol{\zeta}_m \boldsymbol{\Psi}_m\right] \otimes \left[\boldsymbol{\zeta}_m \boldsymbol{\Psi}_m\right] \boldsymbol{\lambda}_m^{-1} + \mathrm{Var}\left[\boldsymbol{\zeta}_v\right]\left[\left[\boldsymbol{\Psi}_m\right] \otimes \left[\boldsymbol{\Psi}_m\right]\right] \boldsymbol{\lambda}_m^{-1} \tag{33}$$

From the equation above, the summation of the column generates the effective independence distribution vector for each element indicates the contribution of a DOF to the linear independence. The DOF that has the lowest contribution to the linear independence is eliminated. The whole procedure is repeated until the number of DOFs meets the given number of target modes.

3.4 Case Study

The method suggested in the previous section is demonstrated here by applying it to a two-dimensional truss bridge whose Young's modulus is set to be a random variable. The result is compared with the existing sensor selection method that is based on Monte Carlo simulation.

3.4.1 Truss Bridge Structure

To demonstrate stochastic EFI, a truss bridge structure was modeled by the finite element method. It is shown in Figure 3-3. The truss bridge is composed of the 41 truss elements and 18 nodes. Each node has two DOFs that describe *x*- and *y*-direction displacement, respectively. The *x*-direction DOF for the *n*th node is numbered 2(*n*-1), and the y-direction DOF is numbered 2*n*. The DOFs of both directions at node 1 and in the y-direction at node 17, that is, DOFs 1, 2, and 34 are constrained. The cross-sectional area of the truss element is 5×10^{-3} m^2, and the mass density is 2500 kg/m^3. The Young's modulus is set to be a random variable that has the truncated normal distribution with mean 70 GPa. Three different standard deviations of the Young's modulus are simulated for verification of the suggested method; 0.0.5×70 GPa, 0.1×70 GPa, and 0.2×70 GPa.

In this case study, the target modes are set to be the first ten modes to represent the overall structural behavior. However, for the purpose of structural health monitoring, one can choose other modes that are useful for a specific fault. The first 4 modes are shown in Figure 3-4, with their mean and standard deviation that are simulated with the help of the SFEM [30, 31].

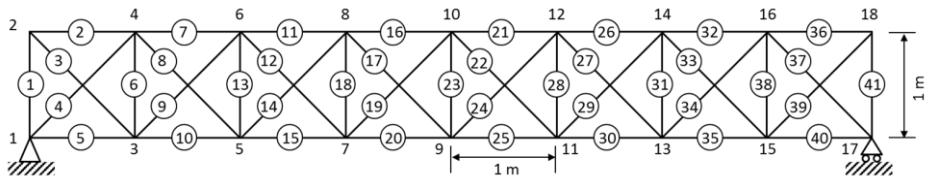

Figure 3-3 Two-dimensional truss bridge.

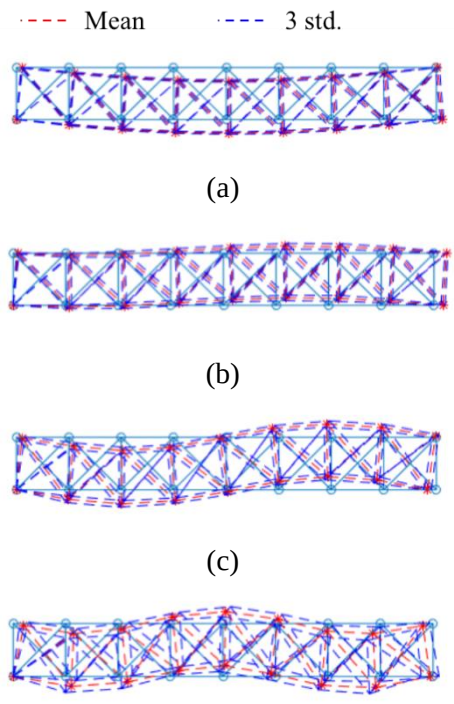

Figure 3-4 Target mode representation with mean and standard deviation: (a) 1st mode, (b) 2nd mode, (c) 3rd mode, and (d) 4th mode.

3.4.2 Sensor Placement Under Uncertainty

3.4.2.1 Monte Carlo Simulation

Optimal sensor selection under parametric uncertainty was studied by Castro-Triguero [20] for a truss bridge. The authors use Monte Carlo simulation to select ten sensors under parametric uncertainty. The histograms of 1,000 EFI simulations of sensor selection under three different variances of the Young's modulus are shown in Figure 3-5.

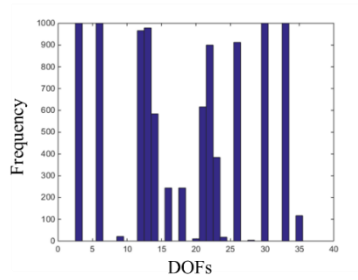

(a)

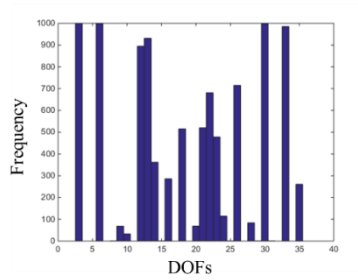

(b)

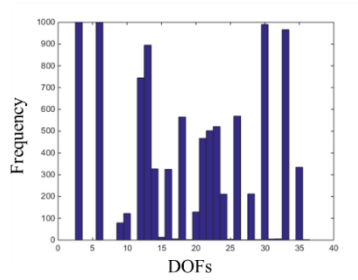

(c)

Figure 3-5 Histograms of 1,000 EFI simulations with stochastic Young's modulus with the mean 70 GPa: (a) the standard deviation 0.05×70 GPa, (b) the standard deviation 0.1×70 GPa, and (c) 0.15×70 GPa.

In Figure 3-5, when the variance of the Young's modulus is low, the set of selected sensors does not change much. However, as the variance increases, the number of sensors consistently selected decreases. For example, DOF 22 is selected for most of the simulation in the lower variance case, but as the variance increases the selection ratio reduces gradually. In contrast to DOF 22, the increase in sensor selection is observed for other sensors such as DOFs 16, 18, and 35. We also observe that the selection of the DOFs around the constraint, such as the DOFs 3, 6, and 33 does not change much even with a high variance of the Young's modulus, because their variances are kept relatively low by the constraints. In contrast, the DOFs away from the constraints, such as DOFs 18, 22, and 23, show less consistency in selection even with the low variance. Similar features are observed for energy-based EFI. The results of strain energy EFI, which uses the stiffness as a weight, are shown in Figure 3-6.

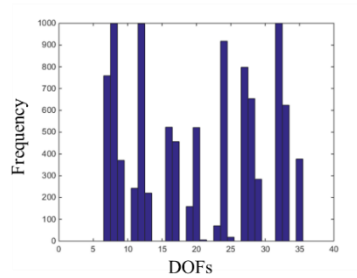

(a)

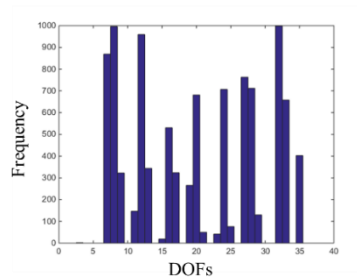

(b)

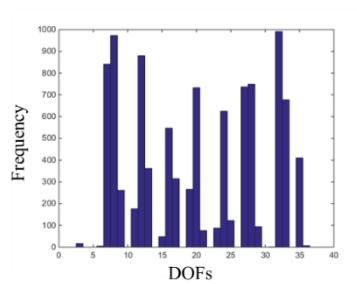

(c)

Figure 3-6 Histograms of 1,000 strain energy EFI simulations with stochastic Young's modulus with the mean 70 GPa: (a) the standard deviation 0.05×70 GPa, (b) the standard deviation 0.1×70 GPa, and (c) 0.15×70 GPa.

Based on the histograms, the MCS method gives the basic idea of selecting sensor locations under parametric uncertainty. The intuitive method is to choose the 10 most frequently selected sensors, for example, in Figure 3-5 (a) the set (3, 6, 12, 13, 14, 21, 22, 26, 30, 33) would be selected. However, this selection does not always assure the optimal set of sensors, especially when the variance is high, because it overlooks the correlation between the sensors. For instance, it is possible that a DOF that has lower linear independence than the DOFs with the 10 highest linear independences is never selected during the simulation, but that it does belong to the 10 highest sensors on average. In the following section, the stochastic EFI indeed shows this case, and finds the optimal sensor locations that give the highest ten linear independences, on average.

3.4.2.2 SEFI Method

The DOFs for the sensor placement are selected using the suggested stochastic EFI for the truss bridge with three different variances. The set of sensors selected using the stochastic EFI are shown and compared with the deterministic EFI and MCS results in Table 3-1.

The performance of each of the three approaches is compared by calculating the determinant of the FIM with respect to the randomly generated 1,000 truss bridges

according to the random property. The histograms of the determinant of the FIM are shown in Figure 3-7 and their mean value is found in Table 3-3.

Table 3-1 The set of 10 sensors selected by EFI using the deterministic EFI, MCS, and stochastic EFI

Std. of Young's modulus, GPa	Method	Sensor set	Mean det($\Phi^T\Phi$) (log scale)
0.05×70	DEFI	3, 6, 12, 13, 14, 21, 22, 26, 30, 33	-107.6160
	MCS		
	SEFI		
0.1×70	DEFI	3, 6, 12, 13, ***14***, 21, 22, 26, 30, 33	-107.6603
	MCS	3, 6, 12, 13, ***18***, 21, 22, 26, 30, 33	-107.7878
	SEFI	3, 6, 12, 13, ***14***, 21, 22, 26, 30, 33	-107.6603
0.15×70	DEFI	3, 6, 12, 13, ***14***, ***21***, 22, 26, 30, 33	-107.7277
	MCS	3, 6, 12, 13, ***18***, 22, ***23***, 26, 30, 33	-107.8264
	SEFI	3, 6, 12, 13, ***14***, ***21***, 22, 26, 30, 33	-107.7277

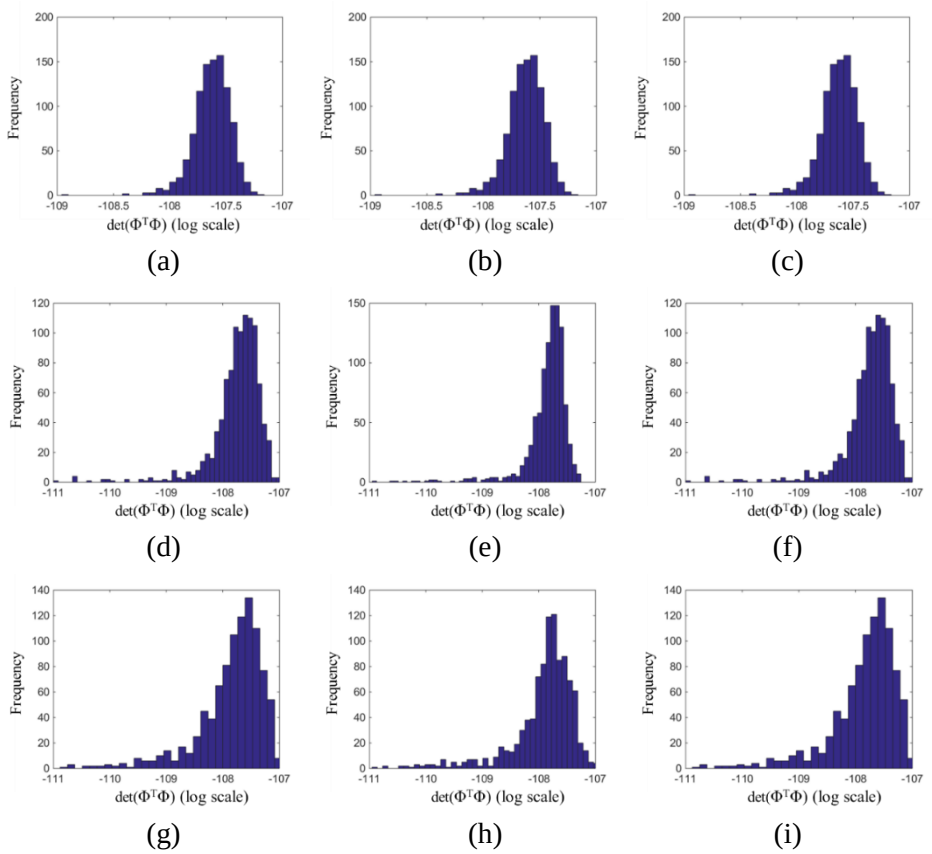

Figure 3-7 Determinant of the Fisher information matrix by (a) EFI with standard deviation of 0.05×70 GPa , (b) MCS with standard deviation of 0.05×70 GPa , (c) stochastic EFI with standard deviation of 0.05×70 GPa , (d) EFI with standard deviation of 0.1×70 GPa , (e) MCS with standard deviation of 0.1×70 GPa , (f) stochastic EFI with standard deviation of 0.1×70 GPa , (g) EFI with standard deviation of 0.15×70 GPa , (h) MCS with standard deviation of 0.15×70 GPa , and (i) stochastic EFI with standard deviation of 0.15×70 GPa.

For the case of a low variance of Young's modulus, the selected sensor sets are not different for between MCS and stochastic EFI. This is because the selected 10 sensors overwhelm the other sensors (Figure 3-4(a)); thus, it is not difficult to choose the sensors using either method. Also, the results are the same with deterministic EFI because of the low variance. However, as the variance increases, the number of overwhelming sensors decreases (Figure 3-4(b)), and the selection becomes confusing when the frequencies in the histogram are similar. However, in this case, the selection of higher frequency does not always give the best result, as mentioned before. For example, in the mid-variance case, the sets selected by the MCS and the stochastic EFI are the same, except for DOFs 14 and 18. Although DOF 14, selected by stochastic EFI, has less frequency than DOF 18, selected by the MCS as in Figure 3-4(b), $\det(\Phi^T\Phi)$ with DOF 14 is higher as shown in Figure 3-7 (b) and in Table 3-3. This phenomenon is intensified as the variance grows, the number of overwhelming sensors decreases, and the difference between the MCS and the stochastic EFI results increases. This is observed in the high-variance case. The number of different sensors between the sets selected by MCS and stochastic EFI increased to two, which are DOF (18, 23) for MCS and (14, 21) for stochastic EFI.

Another aspect to notice is that deterministic EFI gives the same sensor sets as stochastic EFI. This is because deterministic EFI is basically the zeroth order approximation of stochastic EFI. However, deterministic EFI does not always give

the same results as stochastic EFI, if the variance can affect the results more. This will be shown in the results of the following energy-based EFI method. Also, note that the determinant of FIM is decreasing as the variance increases.

The difference in the determinant of the Fisher information matrix, or the linear independence, leads to different estimation performance. To show this, estimations are conducted for two cases of deflection, as shown in Figure 3-8.

For those cases, the Young's modulus of each element is set to have 15% standard deviation from its mean, and 1000 samples are generated accordingly. The corresponding sensor locations are found in Table 3-1. Based on the data measured at the given sensor locations, the deflection for each sample is reconstructed using Eq.(3). Sample estimations for both MCS and proposed method are shown in Figure 3-9. The estimated errors are calculated for 1000 samples; the average differences are shown in Table 3-2.

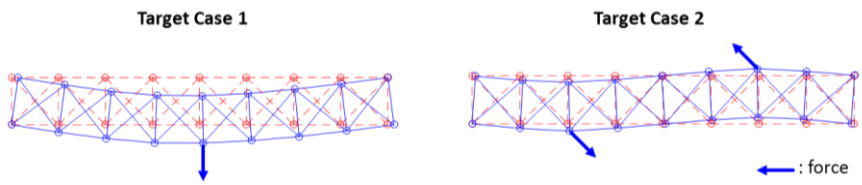

Figure 3-8 The target deflections of a truss bridge with the mean Young's modulus

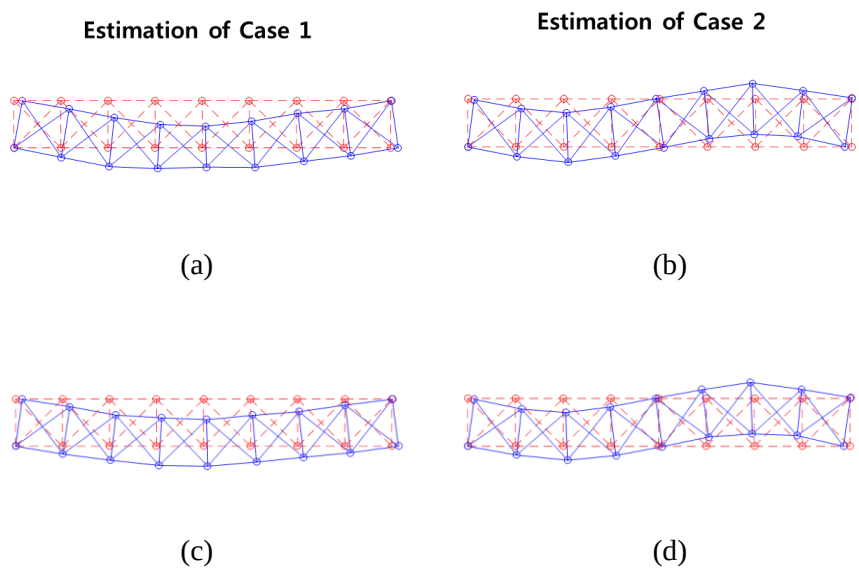

Figure 3-9 The estimated deflection for a randomly generated truss bridge generated by: (a) MCS for case 1, (b) MCS for case 2, (c) SFEM for case 1, and (d) SFEM for case 2

Table 3-2 The average estimation error of MCS and SFEM for given cases

	Average RMS error	
	Case 1	Case 2
MCS	0.0253	0.0055
SFEM	0.0109	0.0023

From the results, we see that the proposed method not only shows the higher linear independence, but also it indeed gives more accurate estimation than the MCS method.

Stochastic EFI is verified with the energy-based method. The stiffness matrix is used for the weight matrix, **W** and the Cholesky decomposition is used to define the FIM. The results are shown in Table 3-3 and the determinant of the FIM for different standard deviations of Young's modulus are shown in Figure 3-10.

Table 3-3 The set of 10 sensors selected by strain-energy-based EFI using the deterministic EFI, MCS, and stochastic EFI

Std. of Young's modulus, GPa	Method	Sensor set	Mean det($\zeta^T\zeta$)
0.05×70	DEFI	8, ***11***, 12, ***16***, ***17***, 24, 27, ***28***, 32, ***33***	4.3139×10^{10}
	MCS	***7***, 8, 12, ***16***, ***20***, 24, 27, ***28***, 32, ***33***	4.3066×10^{7}
	SEFI	***7***, 8, ***9***, 12, ***20***, 24, 27, ***29***, 32, ***35***	9.0426×10^{10}
0.1×70	DEFI	8, ***11***, 12, ***16***, ***17***, 24, ***27***, ***28***, 32, ***33***	4.4851×10^{10}
	MCS	***7***, 8, 12, ***16***, ***20***, 24, ***27***, ***28***, 32, ***33***	1.5199×10^{8}
	SEFI	***7***, 8, ***9***, 12, ***20***, ***23***, 24, ***29***, 32, ***35***	1.5042×10^{11}
0.15×70	DEFI	8, ***11***, 12, 16, ***17***, 24, 27, 28, 32, 33	4.5497×10^{10}
	MCS	***7***, 8, 12, 16, ***20***, 24, 27, 28, 32, 33	3.7275×10^{8}
	SEFI	8, ***11***, 12, 16, ***17***, 24, 27, 28, 32, 33	1.3712×10^{11}

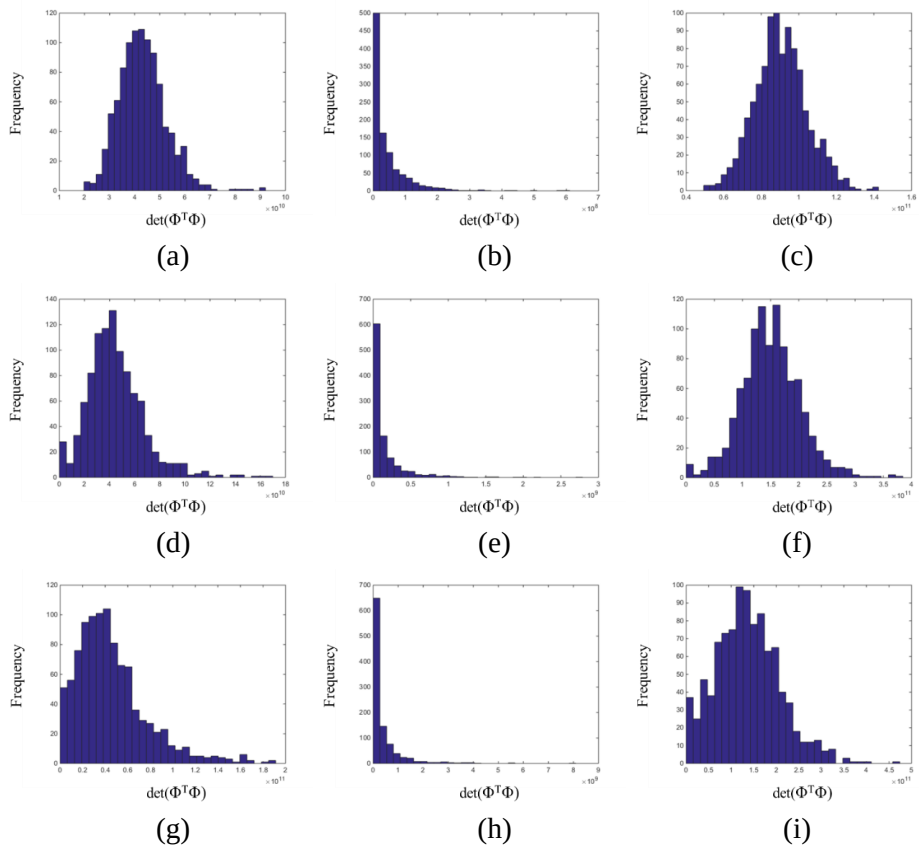

Figure 3-10 Determinant of the Fisher information matrix by (a) energy-based EFI with standard deviation of 0.05×70 GPa , (b) MCS with standard deviation of 0.05×70 GPa , (c) stochastic EFI with standard deviation of 0.05×70 GPa , (d) energy-based EFI with standard deviation of 0.1×70 GPa , (e) MCS with standard deviation of 0.1×70 GPa , (f) stochastic EFI with standard deviation of 0.1×70 GPa , (g) energy-based EFI with standard deviation of 0.15×70 GPa , (h) MCS with standard deviation of 0.15×70 GPa , and (i) stochastic EFI with standard deviation of 0.15×70 GPa.

Unlike the EFI method, this strain-energy-based method shows different sensor selection even in the case of low variance. This is because the stiffness matrix is the function of the random variable, Young's modulus, and the sensor selection becomes more sensitive by taking it into the FIM. Note that while all the methods give different results, stochastic EFI gives the best results among them.

Another energy-based method, the kinetic-energy-based method that uses the mass matrix as the weight matrix, shows different sensor locations with the EFI and strain-energy-based methods due to the targeting of different information. The results are shown in Table 3-4. It is worth noting that the variation of sensor locations according to the uncertainty is more comparable with the EFI method than the strain-energy-based method. This is because the mass matrix is not a random quantity, and does not add randomness to the kinetic energy form as the stiffness matrix does to the strain energy form. Thus, the mode shape matrix is the only factor that affects the result, as seen in the EFI method.

Table 3-4 The set of 10 sensors selected by kinetic-energy-based EFI using the deterministic EFI, MCS, and stochastic EFI

Std. of Young's modulus, GPa	Method	Sensor set	Mean det($\zeta^T\zeta$)
0.05×70	DEFI	8, ***11***, 12, ***16***, ***17***, 24, 27, ***28***, 32, ***33***	4.3139×10^{10}
	MCS	***7***, 8, 12, ***16***, ***20***, 24, 27, ***28***, 32, ***33***	4.3066×10^{7}
	SEFI	***7***, 8, ***9***, 12, ***20***, 24, 27, ***29***, 32, ***35***	9.0426×10^{10}
0.1×70	DEFI	8, ***11***, 12, ***16***, ***17***, 24, ***27***, ***28***, 32, ***33***	4.4851×10^{10}
	MCS	***7***, 8, 12, ***16***, ***20***, 24, ***27***, ***28***, 32, ***33***	1.5199×10^{8}
	SEFI	***7***, 8, ***9***, 12, ***20***, ***23***, 24, ***29***, 32, ***35***	1.5042×10^{11}
0.15×70	DEFI	8, ***11***, 12, 16, ***17***, 24, 27, 28, 32, 33	4.5497×10^{10}
	MCS	***7***, 8, 12, 16, ***20***, 24, 27, 28, 32, 33	3.7275×10^{8}
	SEFI	8, ***11***, 12, 16, ***17***, 24, 27, 28, 32, 33	1.3712×10^{11}

The advantage of stochastic EFI does not only lie in optimal sensor selection, but also in reducing the computational effort. Stochastic EFI requires much less computational work than the MCS method. The MCS method generates a large number of input samples and simulates as many times as the number of the input samples to obtain the probabilistic characteristics of the output. Unlike MCS, stochastic EFI with SFEM needs only one simulation to determine the stochastic properties of the output. The computational times of both methods are compared for the various lengths of the truss bridge in Table 3-5.

Table 3-5 The simulation time of MCS with 1,000 simulations and stochastic EFI for a 2-D truss bridge

No. of truss block	6	7	8	9	10	11
MCS	3.8261	4.8313	5.6736	6.6168	7.5172	8.3789
Stochastic EFI	0.0087	0.011	0.0158	0.0121	0.0161	0.0154

For a six truss block sample, the MCS method with 1,000 simulations takes almost 440 times longer than the proposed method. This computational difference increases if the structure becomes large and complicated, as observed in Table 3-5. As the number of the truss blocks increases, the computational time of MCS increases, while the computational time of the stochastic EFI method remains almost constant. If the required number of samples increases due to multiple random variables, or a complex probability distribution, the computational difference will be much more severe.

3.5 Conclusion

The research described in this dissertation proposed an analytic method for optimal sensor placement under parametric uncertainty. The stochastic EFI was derived, which is composed of the deterministic EFI and an additional random part. With the help of SFEM, the stochastic moments required for the stochastic EFI method are readily obtained, dramatically reducing the total computation time. Applying the suggested method to a 2-dimensional truss bridge case study showed the same or higher determinant of FIM on average as the MCS method, which indicated higher linear independency between the columns of the mode shape matrix with reduced DOFs. It also showed higher representativeness of the general vibration

using the information from the given locations of the sensors. For small variances of the parameter, the selected sensor sets were the same for both methods; however, as the variance increased, the sensor set from the suggested method showed higher linear independence.

The proposed method was expanded to energy-based OSP methods, such as the kinetic energy method, and the strain energy method – both originate from the EFI method. The derivation of such methods for a stochastic case were obtained and they were validated with the same truss bridge case study. The results show that the suggested method shows higher linear independence.

In deriving the stochastic EFI, the symmetric probability distribution of a random variable, and the first-order Taylor expansion for some variables were assumed. For more accurate results, analysis of these assumptions will be required. This analysis will be dealt with in a future study.

Chapter 4. Robust Sensor Network Design

This chapter proposes a sensor network design that considers possible sensor malfunctions, and where the designed sensor network is applied for estimation of the temperature distribution of a Li-ion battery pack. Section 4.1 describes the development of the thermal model for the battery pack to extract the basis matrix. In the next section, an objective function is proposed and solved using the genetic algorithm for the optimization problem that maximizes the linear independence of the system under malfunction. In the final section, the proposed method is validated for various heat conditions.

4.1 Battery System

4.1.1 Battery Pack Overview

Here, a thermal simulation model for a battery pack is developed using the lumped parameter. The battery pack is composed of 50 number 18650 cylindrical cells (ICR18650B4, LG Chem.) with 2600mAh capacity, and 3.7V nominal voltage. The geometry of the battery pack is shown in Figure 4-1(a) and its lumped finite element model is shown in Figure 4-1(b). Each cell is represented as a node and it is connected with the surrounding cells by thermal resistance. At each cell, heat is

generated by electrochemical reactions. The heat is transferred to the surrounding cells by conduction and to the air by convection. The energy balance equation for the *i*th cell in the battery pack is as follows [32-34]:

$$C_h \frac{dT_i}{dt} = R_t \sum_j (T_i - T_j) + \dot{Q} + h(T_i - T_{amb,i}) \tag{34}$$

where C_h is the heat capacity of the cell, T_i is the temperature at the *i*th cell, and T_j is the cell around the *i*th cell, $T_{amb,i}$ is the ambient temperature, t is the time, R_t is the thermal resistance between cells, $\dot{Q}$ is the heat generation rate, and h is the heat transfer coefficient. The rationale for the simplicity of this lumped model is based on three perspectives. First, for practical use in a management system, the computational requirement needs to be small. Second, the errors that could occur in the model can be compensated for through the measurements. In addition, the small size of the 18650 cells with small Biot numbers allow us to assume a small temperature variance in the cell [34, 35].

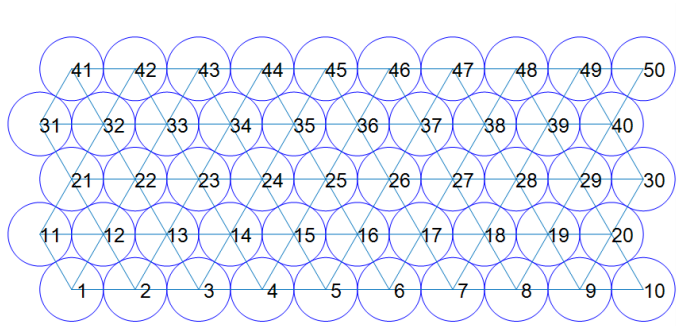

(a)

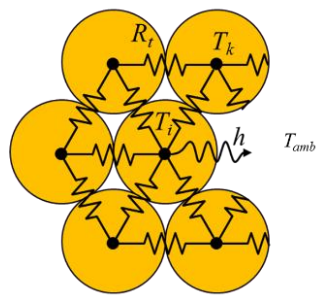

(b)

Figure 4-1 (a) Battery pack geometry, and (b) the lumped parameter model.

4.1.2 Heat Generation Model

During charging and discharging, heat is generated inside the cell. There are several heat sources, such as irreversible ohmic heating, reversible entropic heat, heat from phase change of the active materials, and the heat of mixing [34-36]. In this study, two dominant heat sources, irreversible ohmic heating and reversible entropic heating are considered [32]. The heat generation rate is given as

$$\dot{Q} = I^2 R + IT \frac{dV_{\mathrm{OCV}}}{dT} \tag{35}$$

where I is the input current, R is the impedance of the cell, and V_{OCV} is the open circuit voltage. The first term is the ohmic heating and the second term is the entropic heat. Since the impedance is dependent on the state-of-charge (SOC), the hybrid pulse power characterization (HPPC) test is performed to obtain the SOC and impedance relationship [36, 37]. Figure 4-2(a) shows the HPPC test profile. The discharge pulse is applied for 10 seconds followed by 1C discharge to reduce the SOC by 10%. By repeating this procedure, the impedance at every 10% SOC can be calculated. At the last step, the discharge current is half of the others in order not to violate the cut-off voltage. Therefore, the impedance obtained at this step is for 5% SOC. The impedance is simply calculated as V/I at the beginning of discharging the current. The impedance to the SOC is shown in Figure 4-2(b). Also, dV_{OCV}/dT for

entropic heat is obtained as a function of SOC according to [32, 36]. The voltage of the battery at rest is measured with the change of the temperature at a certain SOC level. The equation V_{OCV}=A+BT+Ct is fitted to the measured voltage, then the coefficient B is dV_{OCV}/dT at a given SOC. The test profile at SOC 0% is shown in Figure 4-3(a) as an example. Similarly, dV_{OCV}/dT at different SOC levels is obtained, and the results are shown in Figure 4-3(b).

Finally, for calculation of the SOC during operation, the coulomb counting method given in Eq.(36) is used [38].

$$z_{k+1} = z_k - \left(\frac{\eta_i \Delta t}{C_n} \right) I_k \tag{36}$$

In the above equation, k is the time index, z_k is the SOC at time index k, η_i is the Coulombic efficiency, Δt is the time difference between k+1 and k time indices, C_n is the nominal capacity of the cell, and I_k is the input current. With the impedance, dV_{OCV}/dT, and SOC as a lookup table, the heat generation can be calculated.

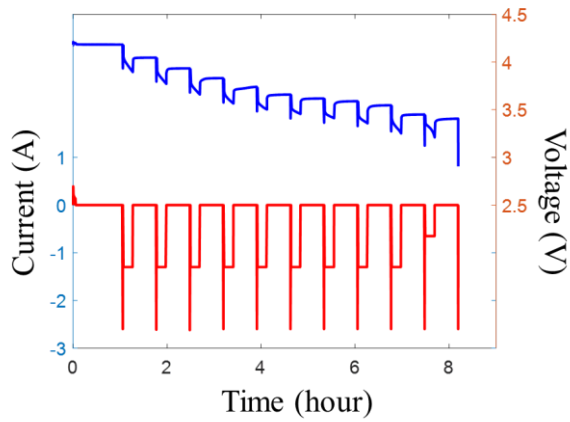

(a)

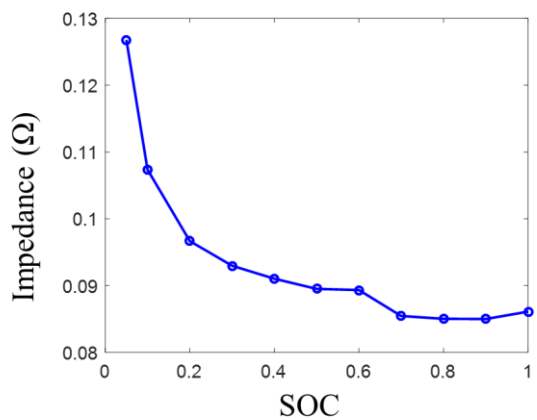

(b)

Figure 4-2 (a) HPPC test profile, and (b) impedance values at SOC levels.

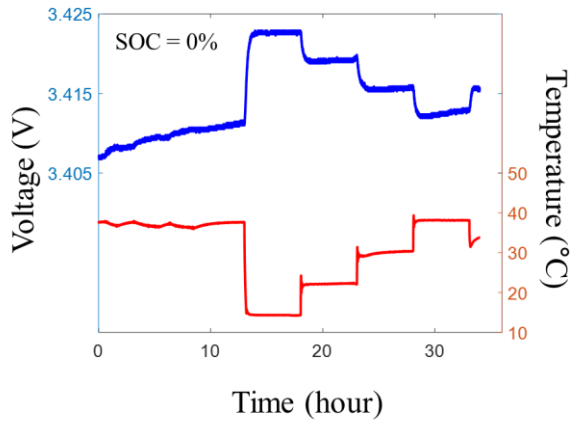

(a)

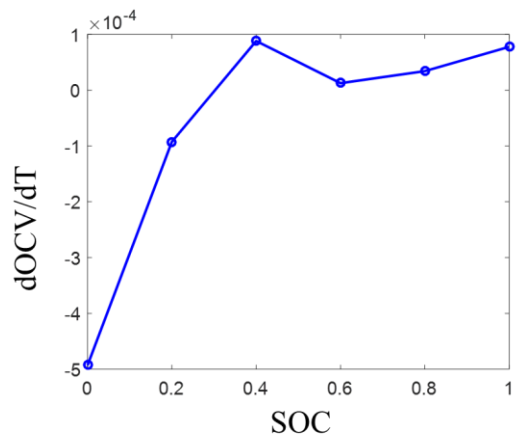

(b)

Figure 4-3 (a) Entropic heat test profile and (b) dV_{ocv}/dT.

4.1.3 Model Calibration and Validation

The model parameters of a single cell, the heat capacity, and the heat transfer coefficient, are calibrated and validated with experimental results. All the experiments are conducted using the Maccor Series 4000 for dis/charging, and the heat chamber for controlling the ambient conditions. First, for model calibration, the temperature under a 1C discharging condition is obtained and used for target vector to optimize the model parameters. The optimized heat capacity and heat transfer coefficient are 69.43 J/K, and 0.1555 W/m^2K, respectively. The measured and the simulated temperatures are shown in Figure 4-4. The model is then validated with the urban dynamometer driving schedule (UDDS) current profile, which is shown in Figure 4-5(a). The UDDS profile and 10% SOC discharging is performed alternatively until the SOC is near zero, then the charging process follows. The measured and the simulated temperatures for this current profile are shown in Figure 4-5(b). The simulated result shows good agreement with the measured temperature during the discharge. The temperature at charging deviates a bit from the measured one, because the impedance used is obtained from discharging pulse. For better results during charging, the impedance needs to be calculated using the charging impulse.

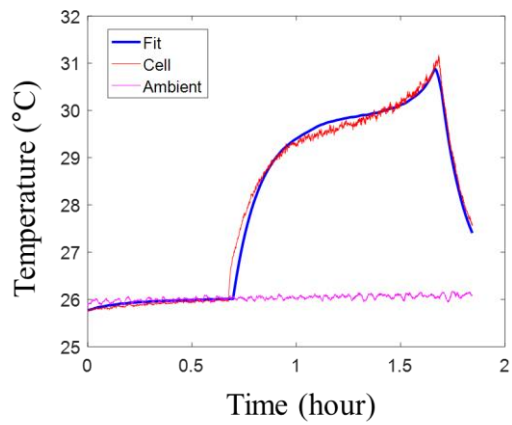

Figure 4-4 The measured and simulated temperatures under 1C (=2.6A) discharge current.

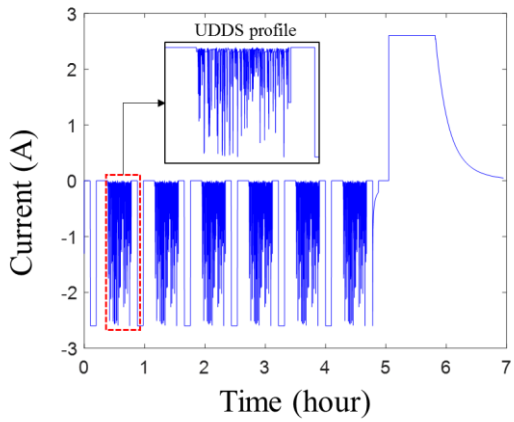

(a)

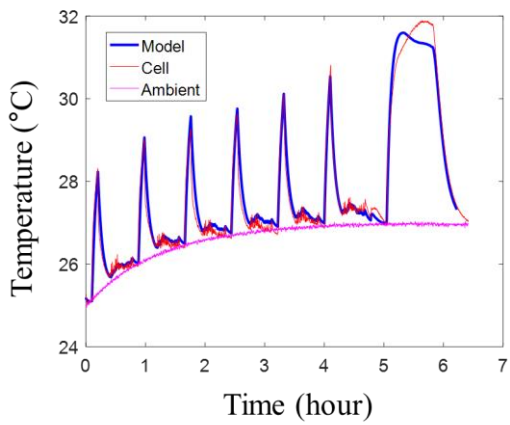

(b)

Figure 4-5 UDDS test results: (a) UDDS current profile, and (b) the measured

4.2 Robust Sensor Network Design

Using the parameters found by the single cell experiments, the pack model is constructed and simulated. Various scenarios that cover possible realizations of the battery pack are generated as a training data set. One of the scenarios is shown in Figure 4-6. It is obtained from the constant current discharge condition. The figure on the left is the temperature change of the cells across time and the figure on the right is the temperature distribution of the pack at a certain time (83 min.). From the training data set, the covariance matrix is found as in Eq.(9), and the eigenanalysis of the covariance matrix gives the basis matrix, $\mathbf{\Phi}$. The first four bases are shown in Figure 4-7. This basis matrix will be used to find the optimal sensor locations.

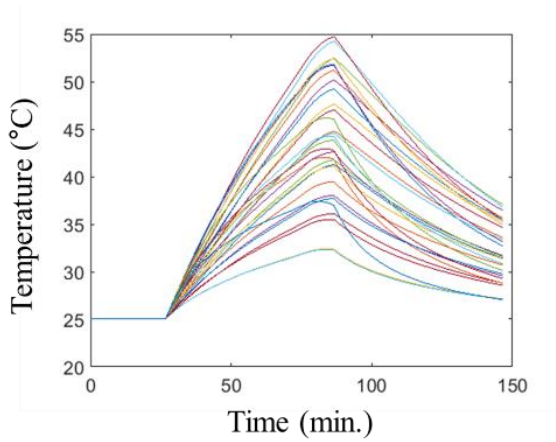

(a)

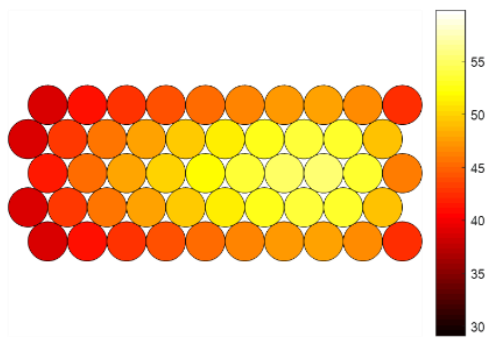

(b)

Figure 4-6 The temperature distribution of a battery pack under constant current: (a) temperature change across time, and (b) the temperature distribution at 83 min.

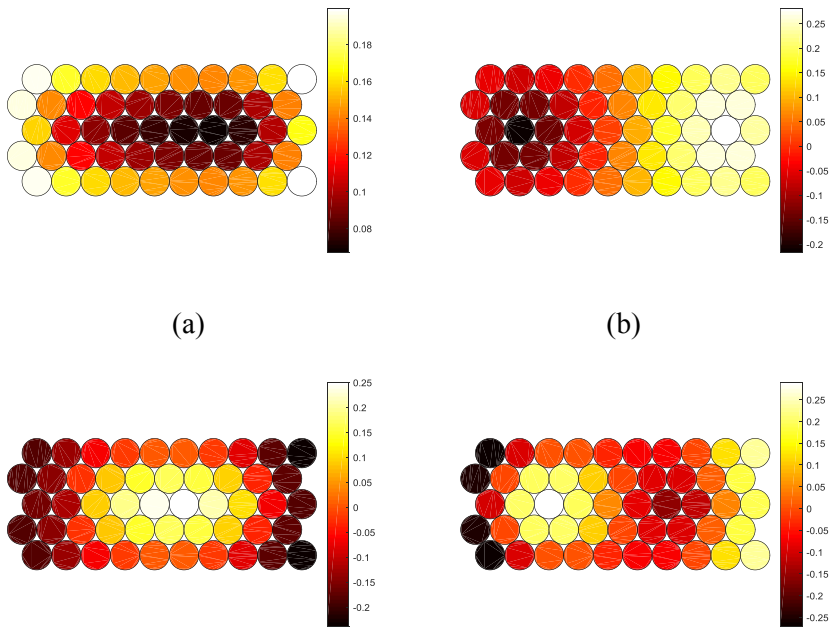

Figure 4-7 The first four eigenvectors of the training data set: (a) 1st mode, (b) 2nd mode, (c) 3rd mode, and (d) 4th mode.

The object of selecting sensor locations is to maximize the determinant of the Fisher information matrix with the (k×k) matrix, $\mathbf{\Phi}_s$. It is the matrix that (n-k) rows and columns are eliminated out of the (n×n) mode shape matrix, $\mathbf{\Phi}$. Therefore, the selections must be made for both rows and columns. The rows are the candidate location of sensor placement and will be decided by the genetic algorithm later. The columns are the mode shape vectors, and will be selected as the mode shapes corresponding to the *k* lowest eigenvalues of $\mathbf{\Phi}$. The choice of low-frequency mode shapes is adequate to represent the general behavior of the system. If the operating condition of the system is restricted so that the dominant mode shapes are known by and large, then the selection of these mode shapes will bring better estimation under that condition. However, this study focuses on the estimation of an arbitrary loading condition and so we stay with k lowest mode shapes.

The choice of rows, or sensor locations, is considered in two aspects. First, the linear independence needs to be high enough to reconstruct the whole thermal map out of the measured signal. Second, for the sensor network to be robust, the sensor network needs to keep its functionality under latent sensor failure. Then, the objective function and the constraints are formulated as follows:

Maximize:

$$f(i_1,...,i_k) = \mathrm{E}[\det(\boldsymbol{\Phi}[\{i_1,...,i_k\}\setminus\{i_j\};1,...,k-1]^{\mathrm{T}}\boldsymbol{\Phi}[\{i_1,...,i_k\}\setminus\{i_j\};1,...,k-1])]$$

Subject to :

$$\det(\boldsymbol{\Phi}[i_1,...,i_k;1,...,k]^{\mathrm{T}}\boldsymbol{\Phi}[i_1,...,i_k;1,...,k]) \geq \alpha\cdot\det(\boldsymbol{\Phi}[i_1^{opt},...,i_k^{opt};1,...,k]^{\mathrm{T}}\boldsymbol{\Phi}[i_1^{opt},...,i_k^{opt};1,...,k])$$

(37)

where k is the given number of sensors, $\boldsymbol{\Phi}[i_1,\ldots, i_k; j_1,..., j_k]$ is the submatrix of $\boldsymbol{\Phi}$ formed from the rows $\{i_1,\ldots, i_k\}$and columns $\{j_1,\ldots, j_k\}$ such that $i_l\in\mathbb{N}$, $1\leq i_l \leq n$, and $i_l \neq i_m$. As mentioned before, the mode shapes are preselected as the first k mode shapes. The random variable for calculating the expectation in the objective function is i_j which is an element in $\{i_1,\ldots, i_k\}$. Therefore, the objective function indicates the average linear independence of the system when a sensor fails. The constraint is set to satisfy a certain performance. That criterion is determined based on the sensor placement result without considering the failure. The i^{opt} is the optimal sensor location when failure is not considered. The coefficient α determines the performance criterion.

Since the sensor placement is the combinatorial problem that selects a given number of sensors k out of n candidate locations, the integer valued optimization method is required. Integer valued optimization is a non-convex problem that cannot be solved by gradient-based optimization. Thus, in this study, the genetic algorithm is adopted to find the sensor location giving the best linear independence of the

system. The genetic algorithm is a sampling-based optimization algorithm inspired by biological evolution. It generates initial random samples (or population) and pass them to the next generation with modification. The modification contains crossover, mutation, and selection that are based on the evaluation of the objective function for the samples. As the generation goes on, the optimal evolution is found as in natural selection [39]. The sensor locations found by the genetic algorithm are shown with the sensor network design that does not consider sensor failure in Figure 4-8.

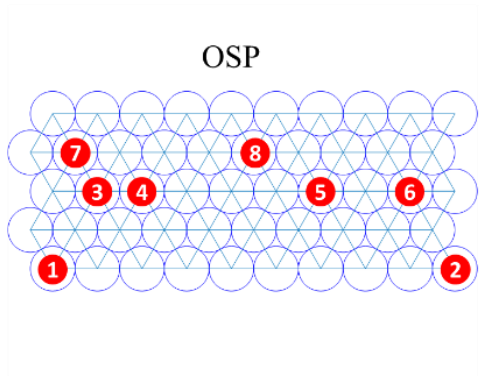

(a)

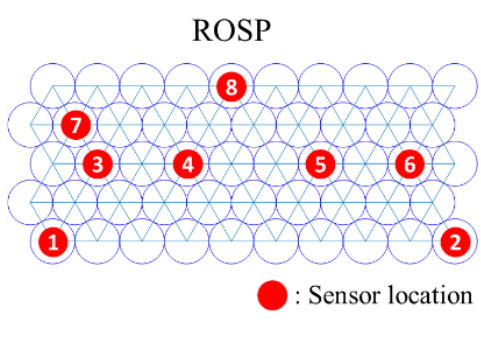

(b)

Figure 4-8 The sensor locations: (a) Optimal sensor placement (OSP), and (b) the robust optimal sensor placement.

4.3 Case Study

The estimation accuracy with and without considering failure of sensors is validated for three test sets. The results are compared with the other sensor network designs; one that does not consider the failure of sensors and another one that uses duplicated sensors for reliability.

4.3.1 Case 1: Different Heat Generation for the Cells

Each cell that makes up the battery pack has a different specification due to manufacturing tolerances and different degradation rates during operation. The first test set is generated to emulate this variation of the cells. The difference in cell specifications emerges as the different heat generation rate. Therefore, each cell is assumed to be discharged with a constant current where the amplitude is realized from the normal distribution N(2.6, 0.26). The temperature change is shown in Figure 4-9(a) and the temperature distribution at 83 min. as shown in Figure 4-9(b) is set as the target temperature distribution to be estimated.

The temperature estimations provided by the existing optimal sensor placement (OSP) method and the proposed robust optimal sensor placement (ROSP) method are compared in Table 4-1. Under normal conditions, both the OSP and the ROSP

methods show accurate estimation results of less than 1°C. Although OSP should have the best estimation result in general, it need not be the best estimation for all cases. This is why ROSP has slightly higher accuracy than OSP for the given case, even though it is not the best sensor network design for the given number of sensors. The accuracy of the estimation decreases as one of the sensors fails. However, the accuracy drop of ROSP is less than that of OSP. Especially when the malfunction occurs on sensor 3 the accuracy drops are severe, but ROSP has less of an accuracy drop than OSP. The same is also true for other cases, except sensors 5 and 7. The results of ROSP with a malfunction of sensor 5 and 7 are also comparable with OSP.

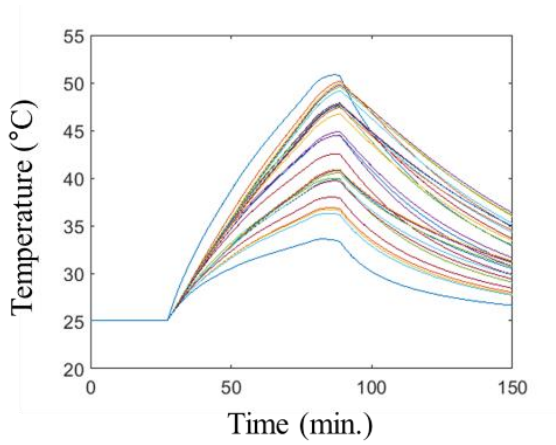

(a)

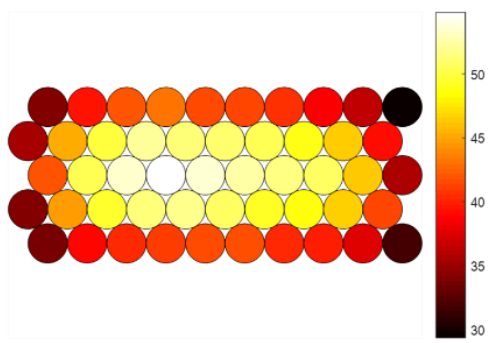

(b)

Figure 4-9 The temperature distribution of the battery pack under a constant current realized from the random distribution: (a) temperature change across time, and (b) the temperature distribution at 83 min.

Table 4-1 The RMS error of OSP and ROSP methods for case 1

Failed sensor No.	Estimation error (RMS)	
	OSP	ROSP
Normal	0.3311	0.5161
1	2.7575	1.4072
2	4.4064	1.2929
3	17.1811	7.6999
4	1.7658	1.6222
5	2.0477	1.974
6	4.8249	2.7842
7	1.6839	1.5953
8	1.9328	1.1974
Mean error for failure	4.57	2.45

4.3.2 Case 2: Forced Convection

The second case is designed to imitate a battery pack with a cooling system. The battery pack is cooled down by forced convection that comes from the left side of the battery pack by a set different heat transfer coefficient for each cell. The simulation result is shown in Figure 4-10. As expected, the cells near the air inlet and the circumference of the pack have a lower temperature than the others.

The estimation results for normal and malfunction conditions are shown in Table 4-2. Similar to what was observed in case 1, both OSP and ROSP methods give accurate estimation results in normal conditions; however, the accuracy drops with a sensor malfunction. The accuracy drop for the ROSP result is less than the accuracy drop for OSP.

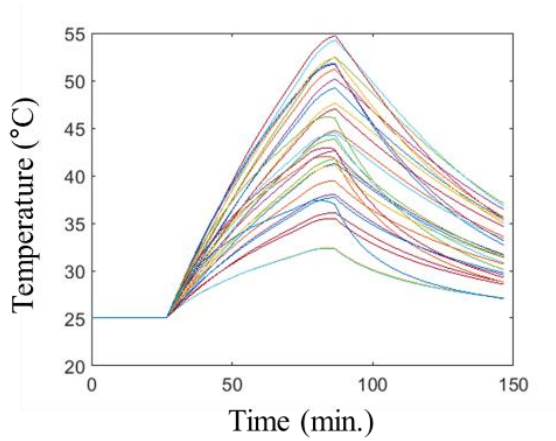

(a)

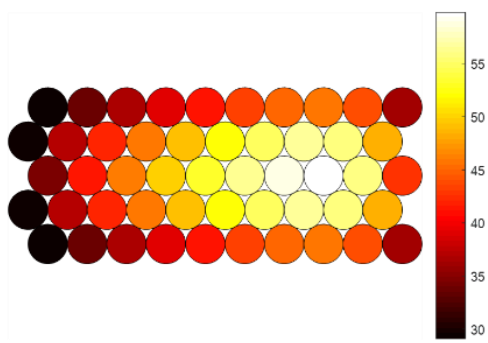

(b)

Figure 4-10 The temperature distribution of a battery pack under forced convection: (a) temperature change across time, and (b) the temperature distribution at 83 min.

Table 4-2 The RMS error of OSP and ROSP methods for case 2

	Estimation error (RMS)	
Failed sensor No.	OSP	ROSP
Normal	0.2658	0.3369
1	3.0945	1.3521
2	5.3976	1.5131
3	20.213	8.2920
4	1.9524	1.7199
5	2.3377	2.0404
6	5.5522	2.8814
7	1.8372	1.5646
8	2.1750	1.1891
Mean error for failure	5.32	2.57

4.3.3 Further Discussion on the Result

This section discusses how two aspects of sensor network design affect the results, specifically, 1) the number of sensors and 2) the selection of mode shapes. First, the impact of the number of sensors is tested by comparing the estimation error along an increasing number of sensors. For case 1 and 2, Table 4-3 shows the relationship between the differing number of selected sensors and the estimation error.

Naturally, as the number of sensors increases the estimation becomes more accurate. Because the number of sensors is the same as the available mode shapes used for estimation, the more sensors used, the accurate the estimation becomes. Another thing to note is that any particular sensor network with a smaller number of sensors is not a subset of a larger sensor network. Thus, the selection of the sensors cannot be conducted in a consecutive manner; rather, it should be conducted for each case.

Table 4-3 Sensor placement corresponding to the number of sensors and estimation accuracy

No. Sensor	Sensor Placement	Estimation Error	
		Case 1	Case 2
5	1, 10, 22, 24, 28	1.9494	2.0523
6	1, 10, 22, 23, 26, 29	1.0888	1.0957
7	1, 10, 22, 24, 27, 29, 32	1.1843	1.1892
8	1, 10, 22, 23, 27, 29, 32, 36	0.3311	0.2658
9	1, 10, 12, 22, 23, 24, 27, 29, 36	0.1491	0.1490
10	14, 20, 22, 23, 25, 28, 32, 37, 41, 50	0.1148	0.1145
11	4, 11, 14, 20, 22, 23, 25, 27, 28, 32, 50	0.0512	0.0511

The second aspect that affects accuracy is the selection of the mode shapes. In the previous study, the mode shapes were successively selected, from the low-order mode shape to the higher order. This way of selecting sensors is for general estimation of the system. However, if the system behavior is confined to a certain range of the domain, estimation accuracy can be enhanced by using the dominant mode shapes in that range. This is verified for case 1 by comparing the results with different mode shapes; one with the low-order mode shape and the other with the dominant mode shape. The result is shown in Table 4-4.

Two things can be observed from these results. First, the estimation accuracy is enhanced by choosing a different mode shape. Although the increase in accuracy observed in this example is not significant due to the small difference between the dominant mode shapes and low-order mode shape, if there are other cases that deviate from the orderly selected mode shape the difference will increase. Second, the sensor locations change as the selected mode shapes are changed. This is because the Fisher information matrix depends on the given mode shape. For this case, it is obvious to find the dominant mode shape, so the sensor network for that specific case is easily found. However, if the cases extend over a wider range, finding the dominant mode shape should be carefully investigated; which will be left for future research.

Table 4-4 Sensor locations and the estimation accuracy for different mode shapes

	Dominant mode shape	Low order mode shape
mode shape	1, 2, 3, 4, 5, 6, 8, 33	1, 2, 3, 4, 5, 6, 7, 8
Sensor locations	1, 4, 12, 20, 22, 23, 26, 28, 41, 50	14, 20, 22, 23, 25, 28, 32, 37, 41, 50
RMS error	0.2854	0.3311

4.4 Conclusion

In this study, we proposed a robust sensor network design that sustains estimation accuracy under failure. We defined the objective function and the constraint for this purpose. The optimization problem was solved by the genetic algorithm. The selected sensor locations were used to reconstruct the temperature distribution of various cases. The estimation results were compared with the other sensor network designs; one was the existing sensor placement method that focuses on accuracy and the other was to use duplicated sensors for robustness. The results show that the proposed method has estimation capability that is comparable to the existing optimal sensor design and that the proposed method has higher reliability than observed using duplicated sensors.

The proposed method is advantageous for practical use in temperature estimation for a battery pack. By combining the model and the measured data, it captures both the computational efficiency and the estimation accuracy. In practice, such as in the case of a battery management system in an electric vehicle, computational efficiency is an important issue. Thus, a complicated model requiring heavy computation cannot be used in spite of its accuracy in estimation. In contrast, the simple model is free from the computational burden; however, it is less accurate. The proposed method requires only a small memory to save the basis matrix and the capability to

calculate the matrix product; inaccuracy is compensated by the measured data and thus, it is suitable for practical use. The use of sensors only to obtain the temperature distribution of the battery pack is not practical because of the cost and the potential for sensor malfunctioning.

Another benefit of the proposed method lies in the sustainability of the sensor network under failure. The sensor network contributes to protect the system as a part of PHM; however, the sensor network itself is vulnerable to failure. Nevertheless, developing another protective system for the sensor network is not a good solution because it requires redundant cost. In this situation, the proposed sensor network design could be a solution because it does not require an extra system, while it does maintain a certain degree of performance under failure. Unlike the PHM, which tries to prevent failure, the proposed design allows the failure and gains time to take care of the failure.

In this study, the sensor locations were found through the optimization method, but it has several shortcomings. It requires significant computational resources to find the optimal solution. Also, to find the proper solution, proper setting of the optimization parameters is important. The genetic algorithm and the other sampling-based optimization methods are known as the global optimization methods; however, their solution depends on the optimization parameters and thus they do not always

give a global optimization solution. Hence, to reduce the computational cost, an analytic solution is required. This will be addressed in future research.

Chapter 5. Contributions and Future Work

5.1 Contributions and Impacts

The work presented in this dissertation focuses on sensor network design for prognostics and health management (PHM). As the beginning step of PHM, the sensor network design has a profound effect on the overall successful implementation of PHM. One of the principal problems in sensor network design is how and where to put the limited number of sensors on the system to have the best information we want to measure. One important property in the sensor network design is the linear independence. The basis vectors of the finite element model that compose an arbitrary behavior of the system, are linearly independent if the signal corresponding to each degree-of-freedom (DOF) is known. However, the limited measure of the system only gives partial information on some measured DOF, as a result, the linear independence between the measured DOF is no longer guaranteed. Since this linear independence determines the representability of the basis vectors for the system, the purpose of the sensor network design becomes to find the locations that make the basis vectors as linearly independent as possible. The maximization of linear independence is considered mainly in two different aspects; it has the following contributions:

Increase in estimation accuracy of sensor network design under system uncertainty

The first research thrust proposes a method to maximize linear independence under system uncertainty. The system in practice always has uncertainty, and the sensor network design will be different from the deterministic solution. To find the optimal sensor network design that considers system uncertainty, the deterministic approach of the sensor network design is modified to its stochastic version. The proposed method is validated using the truss bridge structure, and the results are compared with another stochastic approach, the Monte Carlo simulation method. The results of the research show higher linear independence on average, which means higher representability of the system than observed in the Monte Carlo simulation.

Reduced Computational Cost

By formulating the explicit form of the sensor network design algorithm, the computational cost is greatly reduced. The typical approach to solve the stochastic problem is to use Monte Carlo simulation. However, this sampling-based method generates a large amount of samples and evaluates the system response with respect to the samples; hence, it suffers from a significant computational burden. In contrast,

the proposed method evaluates the stochastic response only once for each iteration. Thus, it reduces the computational time.

Increased Robustness in the Sensing System

Although PHM prevents the system from failure, the sensor network, as a part of PHM, does not have any safety against failure. However, adding another safety system for PHM is too redundant of a design. However, the proposed robust sensor network design could be a compromise. The proposed sensor network is designed to allow and endure the failure to some degree instead of preventing it. Once the failure occurs, the sensor network still does its job with reduced but reasonable performance. This approach increases the robustness of the sensing system without an additional device.

5.2 Suggestions for Future Research

Although the proposed method achieves technical advances in sensor network design, there are still research areas for improvement. Specific suggestions for future research are as follows:

Hybrid Sensor Network Design

This study introduced two primary approaches that are distinguished by the basis vectors of the system. One basis is obtained from the mode shape matrix of the FE model, and the other is from the data. Each method has its own characteristics. The former, called the model-based approach, can estimate all possible realizations of the system; however, for specific cases, the accuracy is less than what is found in the latter, which is called a data-based approach. In contrast, the data-based approach has benefits for estimation of specific cases that are similar to the training data; however, it is less accurate for other cases. Therefore, the model-based sensor network design is relevant and best for unknown and dynamic operating conditions, while the data-based approach is most relevant for predictable operating conditions. However, combination of both methods could give a better solution that lies in between the two approaches.

Sensor Network Design for Transformed Signals

Current sensor networks are designed to estimate the same quantity that the sensor measures. However, for some cases of PHM, the raw signal is transformed to the diagnostic features. For example, the measured signal can be transformed to the entropy form to reveal the health condition of the system. However, sensor network design for the transformed signal has not yet been thoroughly studied, except for the energy form. Therefore, the development of sensor network design for transformed signals will help to improve PHM.

References

[1] M. Pecht, *Prognostics and health management of electronics*: Wiley Online Library, 2008.

[2] J. Lee, F. Wu, W. Zhao, M. Ghaffari, L. Liao, and D. Siegel, "Prognostics and health management design for rotary machinery systems—Reviews, methodology and applications," *Mechanical Systems and Signal Processing,* vol. 42, pp. 314-334, 2014.

[3] A. K. Jardine, D. Lin, and D. Banjevic, "A review on machinery diagnostics and prognostics implementing condition-based maintenance," *Mechanical Systems and Signal Processing,* vol. 20, pp. 1483-1510, 2006.

[4] C. S. Byington, M. Watson, D. Edwards, and P. Stoelting, "A model-based approach to prognostics and health management for flight control actuators," in *Aerospace Conference, 2004. Proceedings. 2004 IEEE*, 2004, pp. 3551-3562.

[5] J. Zhang and J. Lee, "A review on prognostics and health monitoring of Li-ion battery," *Journal of Power Sources,* vol. 196, pp. 6007-6014, 2011.

[6] G. L. Plett, "Sigma-point Kalman filtering for battery management systems of LiPB-based HEV battery packs: Part 1: Introduction and state estimation," *Journal of Power Sources,* vol. 161, pp. 1356-1368, 2006.

[7] G. L. Plett, "Sigma-point Kalman filtering for battery management systems of LiPB-based HEV battery packs: Part 2: Simultaneous state and parameter estimation," *Journal of Power Sources,* vol. 161, pp. 1369-1384, 2006.

[8] G. L. Plett, "Extended Kalman filtering for battery management systems of LiPB-based HEV battery packs: Part 3. State and parameter estimation," *Journal of Power Sources,* vol. 134, pp. 277-292, 2004.

[9] H. Sohn and C. R. Farrar, "Damage diagnosis using time series analysis of vibration signals," *Smart Materials and Structures,* vol. 10, p. 446, 2001.

[10] W. Zhaoxia, L. Fen, Y. Shujuan, and W. Bin, "Motor fault diagnosis based

on the vibration signal testing and analysis," in *Intelligent information technology application, 2009. IITA 2009. Third International Symposium on*, 2009, pp. 433-436.

[11] J. Wang and H. Hu, "Vibration-based fault diagnosis of pump using fuzzy technique," *Measurement,* vol. 39, pp. 176-185, 2006.

[12] K. Shin and J. Hammond, Fundamentals of signal processing for sound and vibration engineers: John Wiley & Sons, 2008.

[13] S. M. Kay, "Fundamentals of statistical signal processing, volume I: estimation theory," 1993.

[14] V. V. Fedorov, *Theory of optimal experiments*: Elsevier, 1972.

[15] D. C. Kammer, "Sensor placement for on-orbit modal identification and correlation of large space structures," *Journal of Guidance, Control, and Dynamics,* vol. 14, pp. 251-259, 1991.

[16] F. M. Hemez and C. Farhat, "An energy based optimum sensor placement criterion and its application to structural damage detection," in *Proceedings-SPIE The International Society for Optical Engineering*, 1994, pp. 1568-1568.

[17] G. Heo, M. Wang, and D. Satpathi, "Optimal transducer placement for health monitoring of long span bridge," *Soil Dynamics and Earthquake Engineering,* vol. 16, pp. 495-502, 1997.

[18] M. Meo and G. Zumpano, "Optimal sensor placement on a large-scale civil structure," in *NDE for Health Monitoring and Diagnostics*, 2004, pp. 108-117.

[19] J. A. Lollock and T. R. Cole, "The effect of mass-weighting on the effective independence of mode shapes," in *46 th AIAA/ASME/ASCE/AHS/ASC Structures, Structural Dynamics, and Materials Conference*, 2005, pp. 1-8.

[20] R. Castro-Triguero, S. Murugan, R. Gallego, and M. I. Friswell, "Robustness of optimal sensor placement under parametric uncertainty," *Mechanical Systems and Signal Processing,* vol. 41, pp. 268-287, 2013.

[21] M. Meo and G. Zumpano, "On the optimal sensor placement techniques for a bridge structure," *Engineering structures,* vol. 27, pp. 1488-1497, 2005.

[22] J. Ranieri, A. Chebira, and M. Vetterli, "Near-optimal sensor placement for linear inverse problems," *IEEE Transactions on Signal Processing,* vol. 62, pp. 1135-1146, 2014.

[23] J. Ranieri, A. Vincenzi, A. Chebira, D. Atienza, and M. Vetterli, "EigenMaps: Algorithms for optimal thermal maps extraction and sensor placement on multicore processors," in *Design Automation Conference (DAC), 2012 49th ACM/EDAC/IEEE*, 2012, pp. 636-641.

[24] D. El Badawy, J. Ranieri, and M. Vetterli, "Near-optimal sensor placement for signals lying in a union of subspaces," in *Signal Processing Conference (EUSIPCO), 2014 Proceedings of the 22nd European*, 2014, pp. 880-884.

[25] M. Kleiber and T. D. Hien, The stochastic finite element method: basic perturbation technique and computer implementation: Wiley, 1992.

[26] M. Kaminski, The stochastic perturbation method for computational mechanics: John Wiley & Sons, 2013.

[27] Z. Yimin, S. Chen, Q. Liu, and T. Liu, "Stochastic perturbation finite elements," *Computers & structures,* vol. 59, pp. 425-429, 1996.

[28] M. Kamiński and M. Kleiber, "Perturbation based stochastic finite element method for homogenization of two-phase elastic composites," *Computers & structures,* vol. 78, pp. 811-826, 2000.

[29] M. K. Pandit, B. N. Singh, and A. H. Sheikh, "Stochastic free vibration response of soft core sandwich plates using an improved higher-order zigzag theory," *Journal of Aerospace Engineering,* 2009.

[30] M. Kamiński, "Generalized perturbation-based stochastic finite element method in elastostatics," *Computers & structures,* vol. 85, pp. 586-594, 2007.

[31] M. Kamiński, "Generalized stochastic perturbation technique in engineering computations," *Mathematical and Computer Modelling,* vol. 51, pp. 272-285, 2010.

[32] C. Forgez, D. V. Do, G. Friedrich, M. Morcrette, and C. Delacourt, "Thermal modeling of a cylindrical LiFePO 4/graphite lithium-ion battery," *Journal of Power Sources,* vol. 195, pp. 2961-2968, 2010.

[33] K. Smith and C.-Y. Wang, "Power and thermal characterization of a lithium-ion battery pack for hybrid-electric vehicles," *Journal of Power Sources,* vol. 160, pp. 662-673, 2006.

[34] S. Al Hallaj, H. Maleki, J.-S. Hong, and J. R. Selman, "Thermal modeling and design considerations of lithium-ion batteries," *Journal of Power Sources,* vol. 83, pp. 1-8, 1999.

[35] B. Schweitzer, S. Wilke, S. Khateeb, and S. Al-Hallaj, "Experimental validation of a 0-D numerical model for phase change thermal management systems in lithium-ion batteries," *Journal of Power Sources,* vol. 287, pp. 211-219, 2015.

[36] K. Onda, H. Kameyama, T. Hanamoto, and K. Ito, "Experimental study on heat generation behavior of small lithium-ion secondary batteries," *Journal of the Electrochemical Society,* vol. 150, pp. A285-A291, 2003.

[37] D. Dees, E. Gunen, D. Abraham, A. Jansen, and J. Prakash, "Electrochemical modeling of lithium-ion positive electrodes during hybrid pulse power characterization tests," *Journal of The Electrochemical Society,* vol. 155, pp. A603-A613, 2008.

[38] G. L. Plett, "Extended Kalman filtering for battery management systems of LiPB-based HEV battery packs: Part 2. Modeling and identification," *Journal of Power Sources,* vol. 134, pp. 262-276, 2004.

[39] M. D. Vose, The simple genetic algorithm: foundations and theory vol. 12: MIT press, 1999.

Abstract (Korean)

기계 시스템 건전성 평가를 위한 효율독립성 기반 센서 네트워크 디자인 연구

김 태 진
서울대학교 대학원
기계항공공학부

기계 시스템의 불시 고장은 경제적, 사회적 손실을 야기한다. 이러한 손실을 미연에 방지하기 위한 방안으로 PHM (prognostics and health management)이 주목받고 있다. PHM 은 시스템의 현 상태를 추정하고 미래 상태를 예측하여 시스템의 고장을 미연에 방지하고 나아가 시스템의 최적 운영을 가능케 한다. PHM 은 측정, 진단, 예지, 그리고 관리의 네 단계로 구성되는데, 특히 측정은 PHM 의 첫 단계로써 이후 단계의 성공적 수행에 결정적 영향을 미친다.

본 연구는 시스템으로부터 최대의 정보를 얻기 위한 센서 네트워크 디자인에 관한 문제를 다룬다. 먼저 시스템의 불확실성을 고려한 센서 네트워크 디자인에 관해, 그리고 센서의 고장을 고려한 센서 네트워크 디자인에 대해 논의한다. 시스템의 불확실성을 고려한 센서 네트워크 디자인은 기존의 결정론적 접근 방식을 변형하여 확률적으로 접근 가능한 식을 유도하였으며 이로부터 기존의 확률적 접근 방식이던 샘플링 기반 방법에 비해 정확도와 효율을 개선할 수 있었다. 다음으로 센서의 고장을 고려함으로써 일부 센서의 고장 시에도 그 역할을 지속할 수 있는 강건한 센서 네트워크 디자인을 제안하여 전체 PHM 의 안전성을 높였다.

주제어 : 센서 네트워크 디자인

유효독립 방법

고유지도 방법

확률적 효율독립 방법

강건 센서 네트워크 디자인

학 번 : 2011-20702